Modelling of CPW Structures for the Characterisation of Thin Film Materials

Konrad Wilczynski,[$] Malgorzata Celuch,[#] Marzena Olszewska – Placha[#]

[$]Faculty of Physics, Warsaw University of Technology, Poland

[#] QWED Sp. z o. o., Poland

Foundation for Polish Science

Presenter: Lukasz Nowicki, **QWED Sp. z o. o.**, Poland

06.07.2022, Limoges

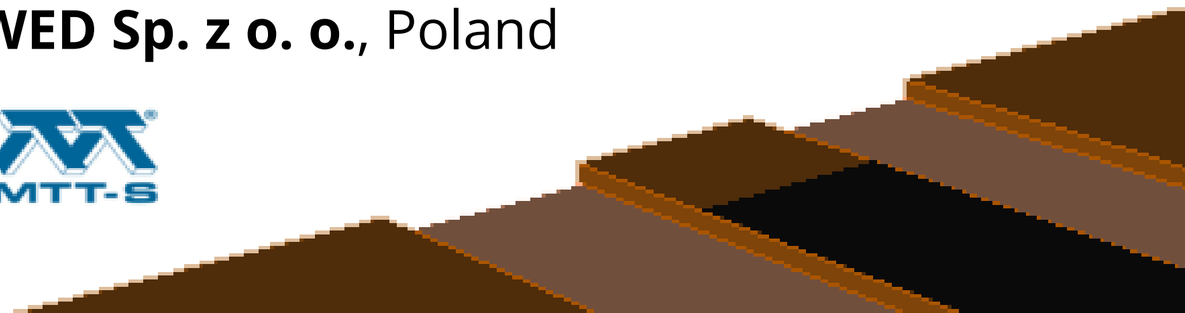

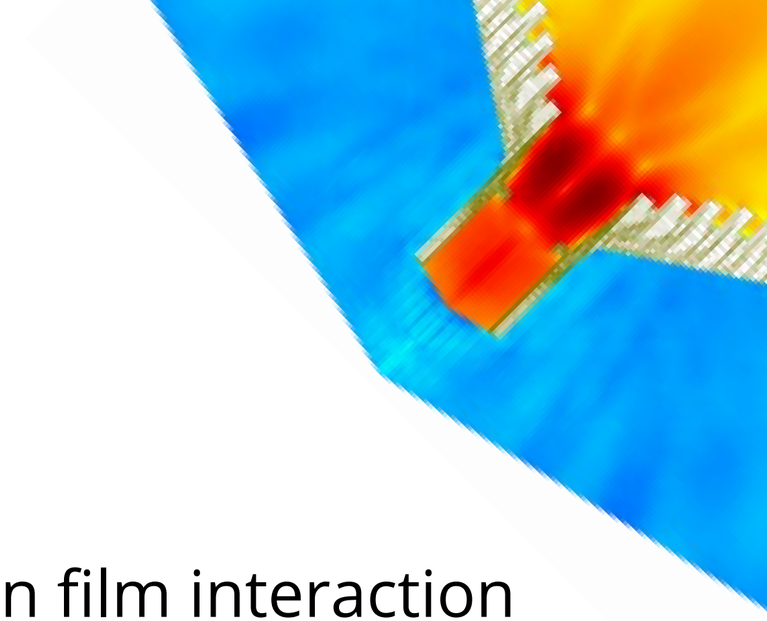

Outline

- Coplanar waveguide structure **CPW**
  - Introducing the basics
  - Which EM parameters meaningfully describe thin film interaction with GHz waves?
- **CPW** modelling with the Finite Difference Time Domain **FDTD** method
  - How does one efficiently model a layer of ultra-small thickness in general purpose electromagnetic **EM** simulators?
- Application of the model to development of a 10 GHz dielectric resonator **DR** scanner for graphene anodes.
- Conclusions

Coplanar waveguide structure CPW

Introduction

Coplanar waveguides are a well-known variety of transmission lines used for example, to propagate of electrical signals with frequencies of the order of gigahertz (microwave range). Due to their simple structure, CPW waveguides are commonly used as elements of integrated microwave circuits.

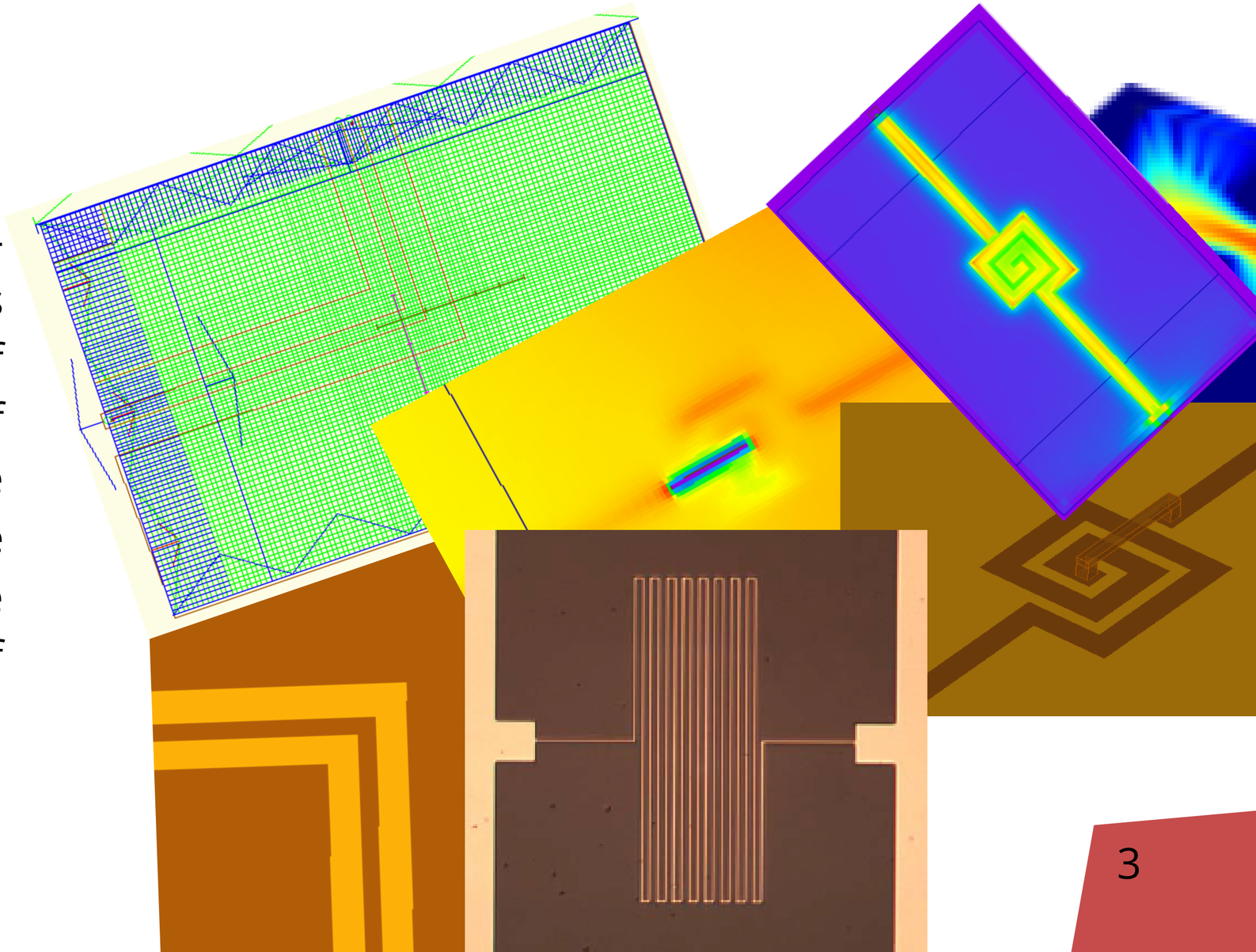

Complex dielectric function

$$\nabla \cdot \boldsymbol{D} = \rho, \quad \nabla \cdot \boldsymbol{B} = 0, \quad \nabla \times \boldsymbol{E} = -\frac{\partial \boldsymbol{B}}{\partial t}, \quad \nabla \times \boldsymbol{H} = \boldsymbol{J} + \frac{\partial \boldsymbol{D}}{\partial t}$$

Maxwell's equations

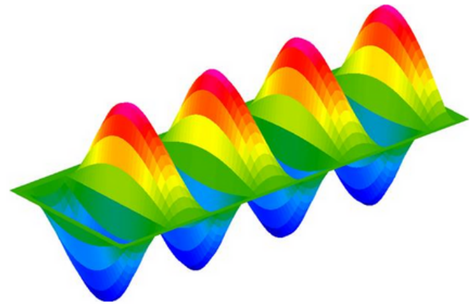

$$X(t) = \tilde{X}(\omega) \cdot e^{j\omega t}$$

$$\nabla \cdot \tilde{\boldsymbol{D}} = \tilde{\rho}, \quad \nabla \cdot \tilde{\boldsymbol{B}} = 0, \quad \nabla \times \tilde{\boldsymbol{E}} = -j\omega \tilde{\boldsymbol{B}}, \quad \nabla \times \tilde{\boldsymbol{H}} = \tilde{\boldsymbol{J}} + j\omega \tilde{\boldsymbol{D}}$$

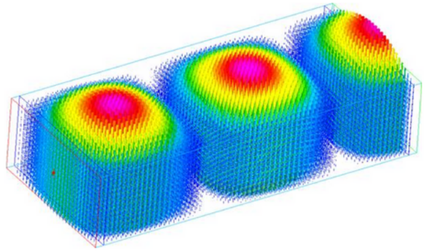

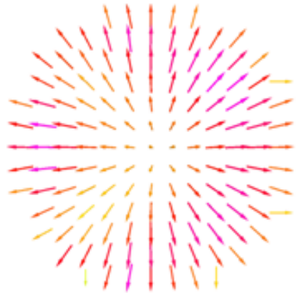

$$\tilde{\boldsymbol{D}} = \varepsilon_0 \tilde{\varepsilon}_r \cdot \tilde{\boldsymbol{E}}, \quad \tilde{\boldsymbol{B}} = \mu_0 \tilde{\mu}_r \cdot \tilde{\boldsymbol{H}}, \quad \tilde{\boldsymbol{J}} = \tilde{\sigma} \cdot \tilde{\boldsymbol{E}}$$

Constitutive equations in EM

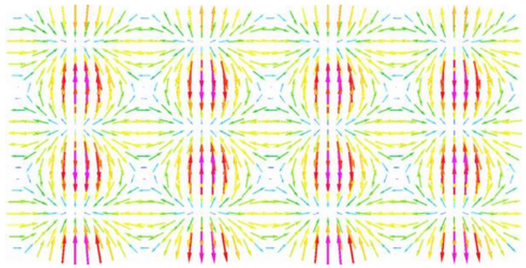

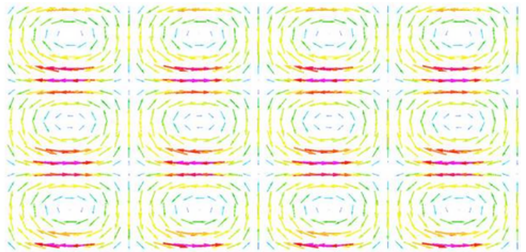

$$\nabla \times \frac{\nabla \times \tilde{\boldsymbol{E}}}{\tilde{\mu}_r} - \omega^2 \mu_0 \varepsilon_0 \left(\tilde{\varepsilon}_r - j\frac{\tilde{\sigma}}{\omega \varepsilon_0} \right) \cdot \tilde{\boldsymbol{E}} = 0, \quad \tilde{\boldsymbol{H}} = \frac{-1}{j\omega \mu_0 \tilde{\mu}_r} \nabla \times \tilde{\boldsymbol{E}}$$

Distributions of electric and magnetic fields

$$\hat{\varepsilon} = \varepsilon' - i\varepsilon''$$

Complex permittivity

Methods for measuring the complex dielectric function

- Parallel Plate
- Coaxial Probe
- Transmission Line
- Free Space
  - Resonators

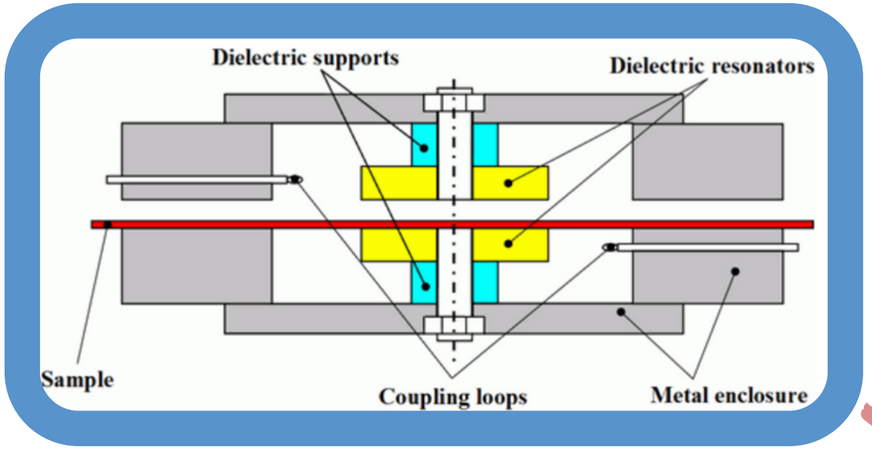

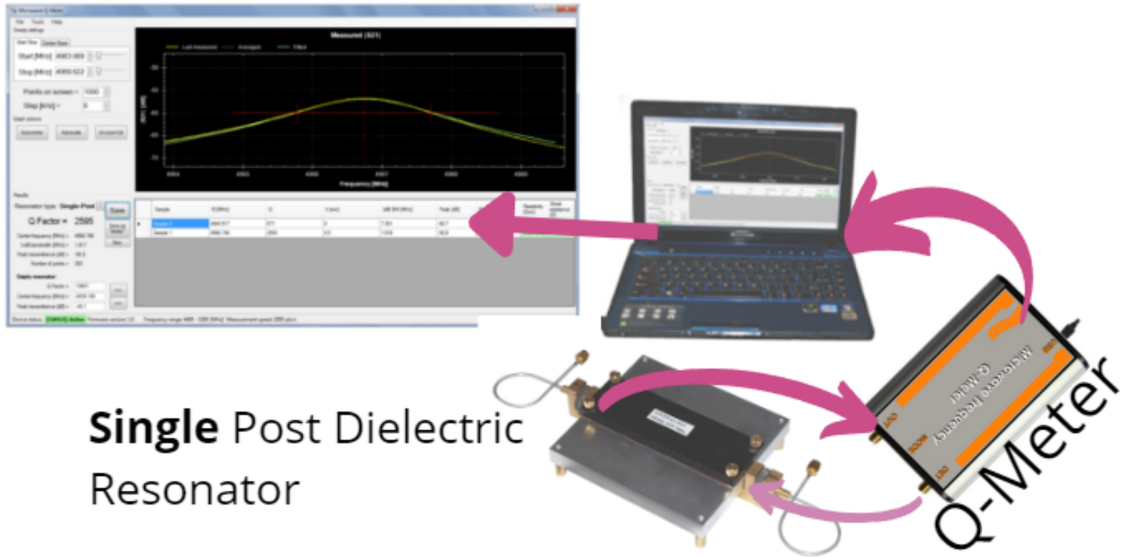

Single Post Dielectric Resonator

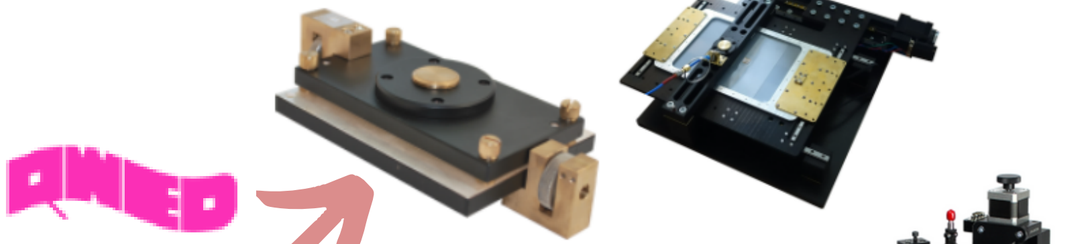

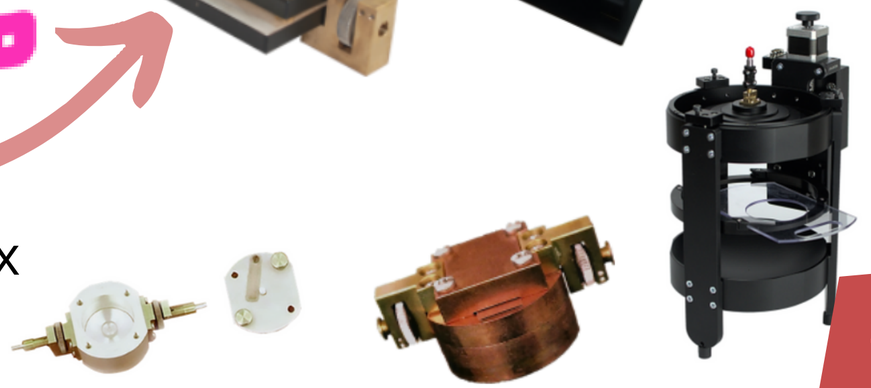

The most common methods for measuring the complex dielectric (and possibly magnetic) function. [6][8]

Description of quasi-TEM waveguides

Distribution of transverse components of electric **E** and magnetic **H** fields

$$\tilde{E}_t(x,y,z) = (c^+ \cdot e^{-\gamma z} + c^- \cdot e^{\gamma z}) \cdot \tilde{e}_t$$

$$\tilde{H}_t(x,y,z) = (c^+ \cdot e^{-\gamma z} - c^- \cdot e^{\gamma z}) \cdot \tilde{h}_t$$

complex propagation constant

$$\gamma = \alpha + j\beta$$

$$\varepsilon_{\mathrm{eff}} = \left(\frac{\beta}{k_0}\right)^2$$

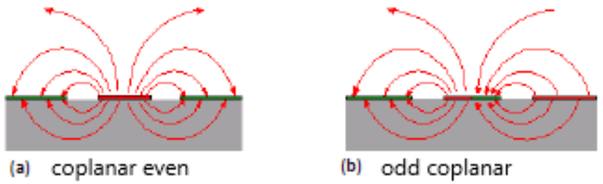

(a) coplanar even (b) odd coplanar

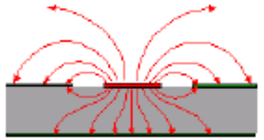

(c) microstrip (parasitic) type

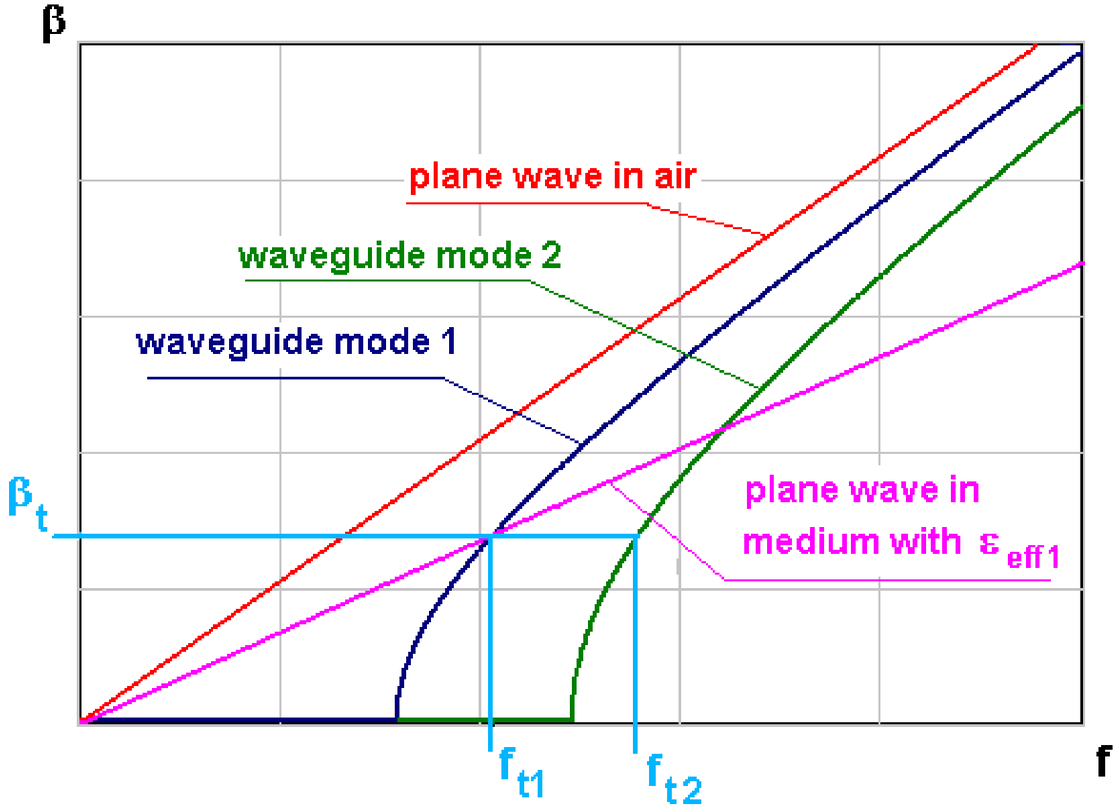

First insight template generation

Description of quasi-TEM waveguides

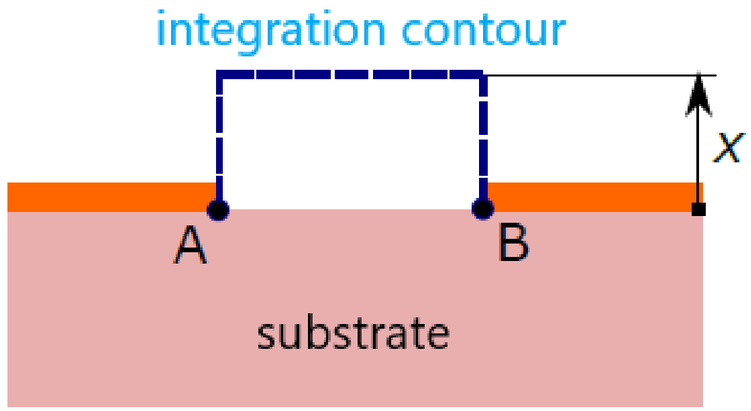

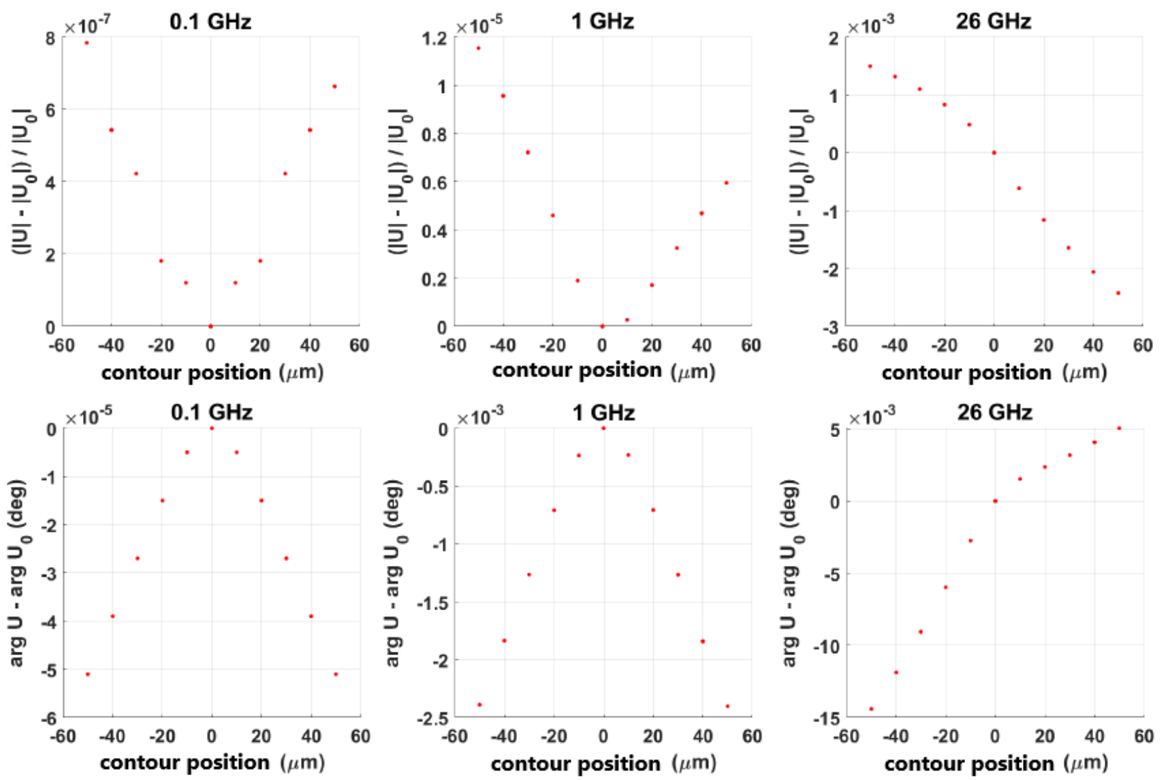

$$v(z) = -\int_A^B \tilde{\boldsymbol{E}}_t(z)\cdot \boldsymbol{dl} \qquad i(z) = \oint_\Gamma \tilde{\boldsymbol{H}}_t(z)\cdot \boldsymbol{dl}$$

$$v_0 = -\int_A^B \tilde{\boldsymbol{e}}_t \cdot \boldsymbol{dl} \qquad i_0 = \oint_\Gamma \tilde{\boldsymbol{h}}_t \cdot \boldsymbol{dl}$$

$$v(z) = (c^+ \cdot e^{-\gamma z} + c^- \cdot e^{\gamma z})v_0 \qquad i(z) = (c^+ \cdot e^{-\gamma z} - c^- \cdot e^{\gamma z})i_0$$

$$Z_0 = \frac{v_0}{i_0}$$

characteristic impedance [6]

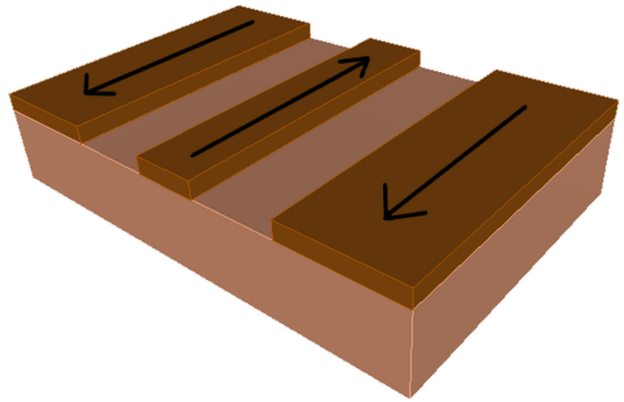

Coplanar waveguide structure CPW

Scattering matrix

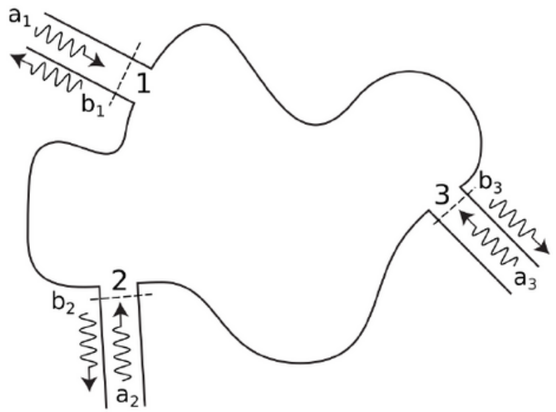

$$a_i = \frac{V_i + Z_i I_i}{2\sqrt{|\Re(Z_i)|}}, \quad b_i = \frac{V_i - Z_i^* I_i}{2\sqrt{|\Re(Z_i)|}}$$

$$P_i = \Re(V_i I_i^*) = |a_i|^2 - |b_i|^2$$

$$\begin{pmatrix} b_1 \\ \vdots \\ b_n \end{pmatrix} = \begin{pmatrix} S_{11} & \cdots & S_{1n} \\ \vdots & \ddots & \vdots \\ S_{n1} & \cdots & S_{nn} \end{pmatrix} \cdot \begin{pmatrix} a_1 \\ \vdots \\ a_n \end{pmatrix}$$

$$Z_i = Z_R = \Re(Z_R)$$

$$a_i = c_i^+ \cdot \frac{v_0}{\sqrt{Z_R}}, \quad b_i = c_i^- \cdot \frac{v_0}{\sqrt{Z_R}}$$

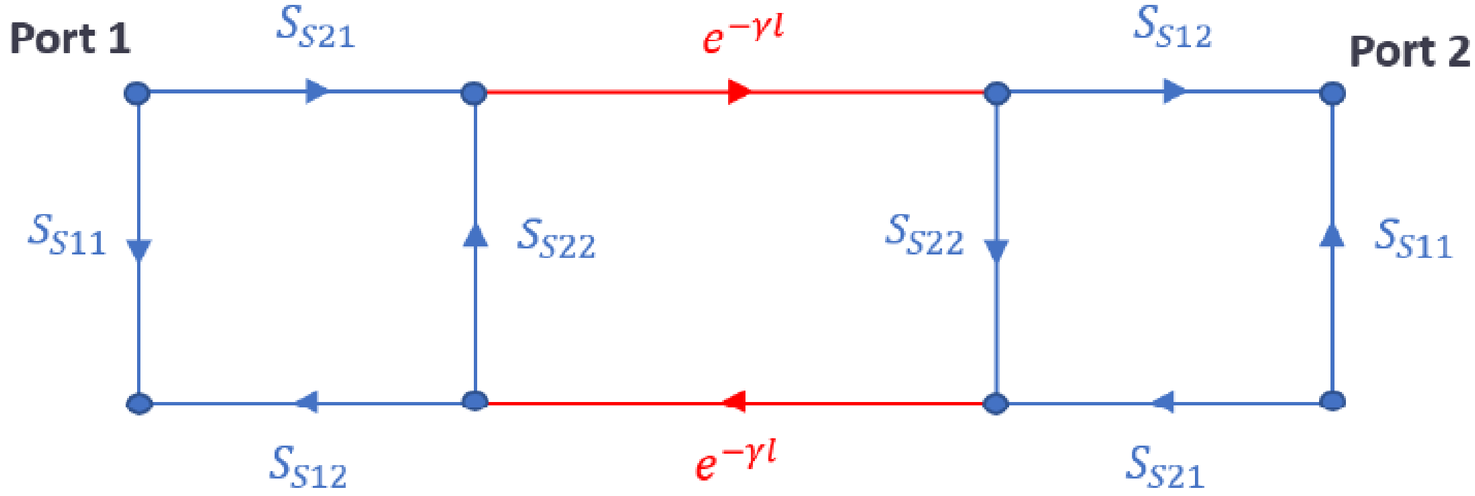

Impedance step $Z_R - Z_0$

CPW segment of length l

Impedance step $Z_0 - Z_R$

$$S_{11} = S_{S11}\frac{1 - e^{-2\gamma l}}{1 - S_{S11}^2 e^{-2\gamma l}} = S_{22}$$

$$S_{21} = (1 - S_{S11}^2)\frac{e^{-\gamma l}}{1 - S_{S11}^2 e^{-2\gamma l}} = S_{12}$$

$$S_{S11} = \frac{Z_0 - Z_R}{Z_0 + Z_R}, \quad S_{S12} = \frac{2Z_R}{Z_0 + Z_R}$$

$$S_{S21} = \frac{2Z_0}{Z_0 + Z_R}, \quad S_{S12} = \frac{Z_R - Z_0}{Z_0 + Z_R}$$

$$Z_0 = Z_R\sqrt{\frac{S_{21}^2 - (1 + S_{11})^2}{S_{21}^2 - (1 - S_{11})^2}}$$

Proposal for measuring thin films

CPW waveguide, as a quasi-TEM guide, is adequate to study interaction of composites with plane electromagnetic waves.

Significant advantages:

- simplicity of the measurement - it is enough to placed directly on the surface of the conductive strips
- low sensitivity of the results to geometric dimensions of the sample

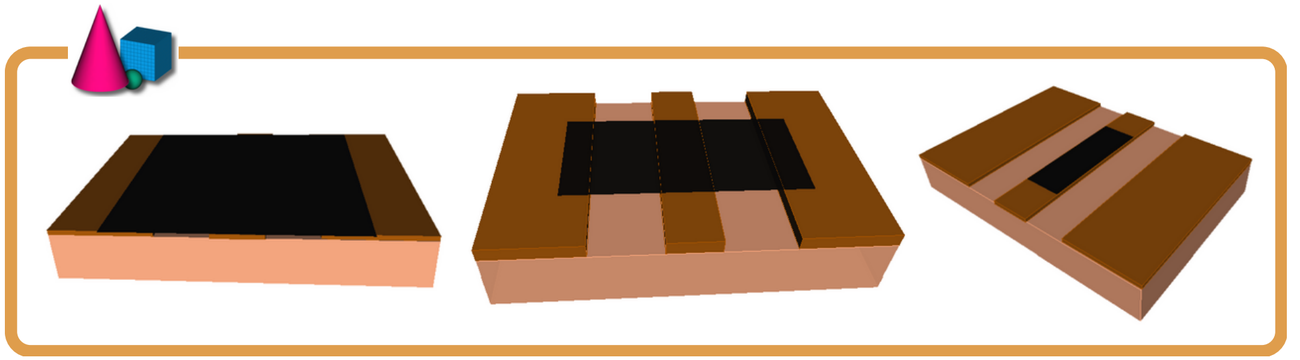

$\hat{\varepsilon} = \varepsilon' - i\varepsilon'' = ?$

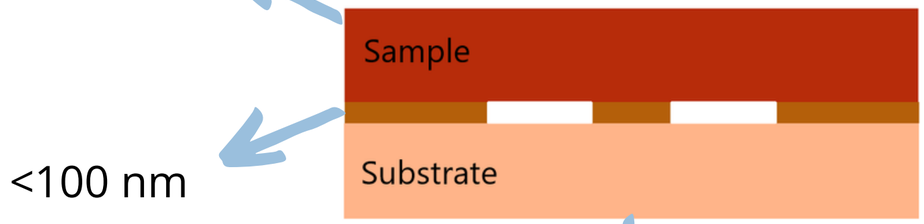

<100 nm

With known and low permittivity $\hat{\varepsilon}$

Which EM parameters meaningfully describe thin film interaction with GHz waves?

$$R_s = (d_0 \sigma_0)^{-1} = (d\,\sigma)^{-1}$$

parameters of the original metal

dielectric surrogate

Scalling:

- Anisotropic
- Impedance-conserving

Specifically, sub-cellular models in conformal FDTD are recommended for the modelling of minimally thin surrogate sheets with acceptable computer effort.

METALLIZATION SHEET RESISTANCE/CONDUCTIVITY

Metallization	$R_{S,DC}$ (Ω/□)	$R_{S,RF}$ (Ω/□)	σ_{DC} (10^7 S/m)	σ_{RF} (10^7 S/m)
5 nm Cr + 10 nm Au	6.86	8.69	0.972	0.767
5 nm Cr + 20 nm Au	2.53	2.91	1.58	1.37
5 nm Cr + 30 nm Au	1.44	1.73	1.98	1.65
5 nm Cr + 50 nm Au	0.710	0.814	2.56	2.23
5 nm Cr + 70 nm Au	0.487	0.528	2.74	2.53
5 nm Cr + 100 nm Au	0.326	0.346	2.92	2.75

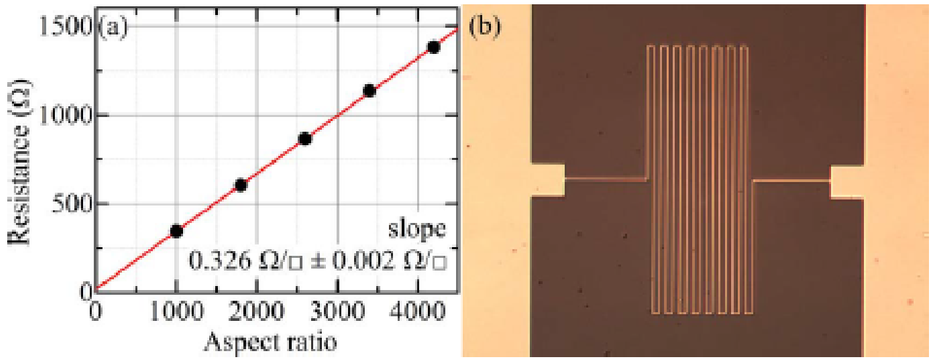

(a) Resistance of the thin metallic strip versus the aspect ratio (length divided by width); slope equals the sheet resistance.
(b) Picture of one of the metallic structures used in the Transfer Length Method for determining the metallization dc sheet resistance for 5-nm Cr + 100-nm Au metallization. [4]

Coplanar waveguide structure CPW

Anisotropic

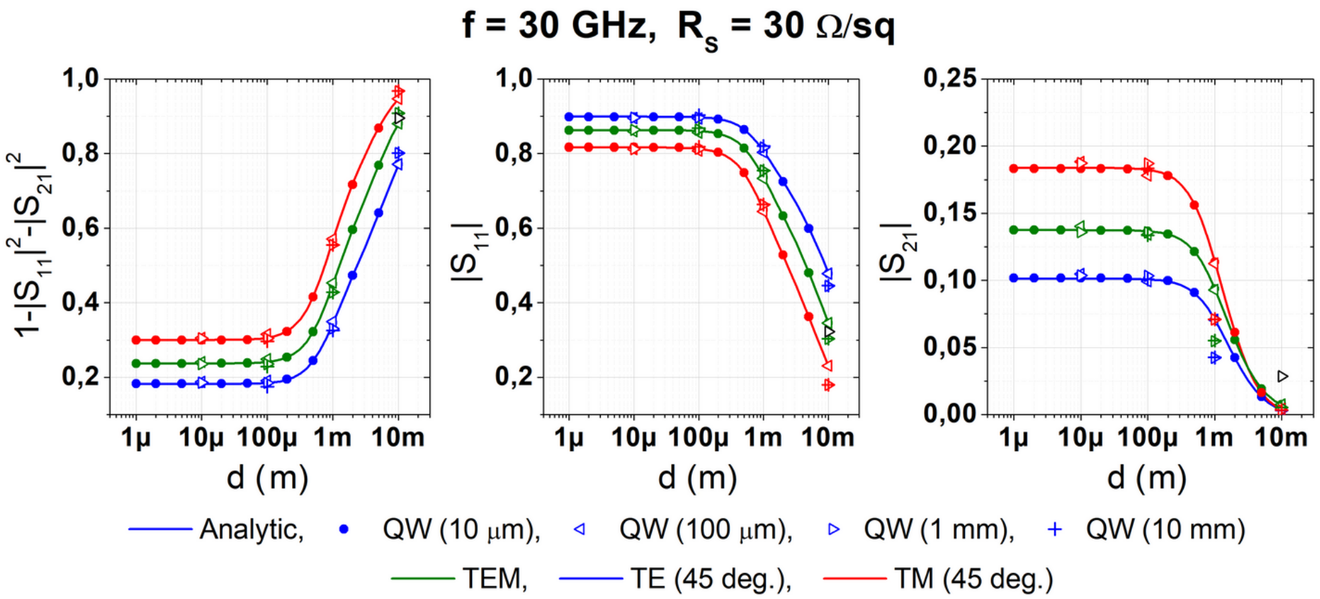

Anisotropic

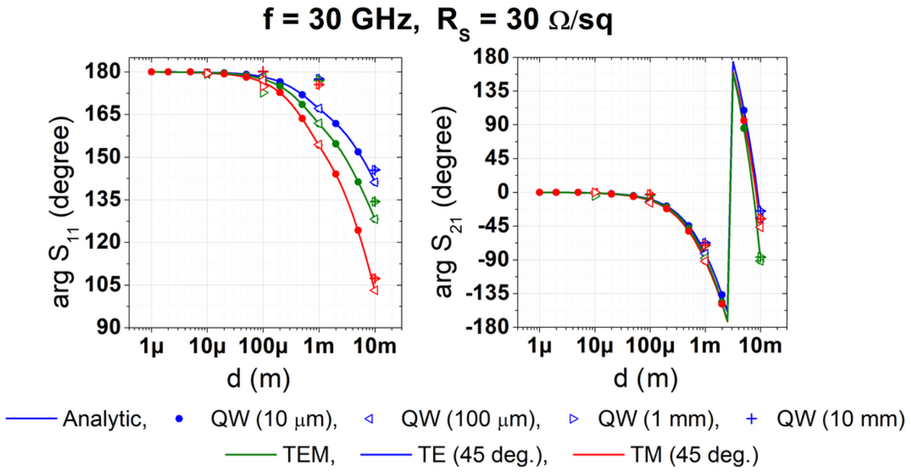

Impedance-conserving

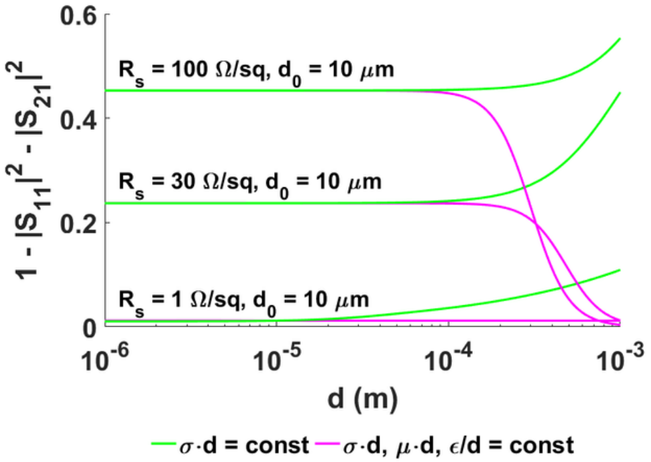

Comparisons of the original metal layers and their scaled surrogates:

- Absorption is retained for surrogates thicker up to d=0.02λ, but nearly doubles when d=0.1λ
- Accuracy is improved by anisotropic scaling, but only for TM waves and thick surrogates (d=10mm, black mark in the figures above).
- Magnitudes as well as phases of reflection (~180°) and transmission (~0°) are retained for d<0.02λ; at d=0.1λ phase difference ca. 10° between the polarisations is caused, which may visibly modify field pattern above and below the surrogate
- Impedance-conserving models allow a broader range of scaling for low-resistance sheets as in aeronautics, but fail for high-resistance susceptors:

CPW modelling with the FDTD method

Introduction

Faraday and Ampere

$$\frac{\partial B_x}{\partial t} = \frac{\partial E_y}{\partial z} - \frac{\partial E_z}{\partial y}$$

$$\frac{\partial B_y}{\partial t} = \frac{\partial E_z}{\partial x} - \frac{\partial E_x}{\partial z}$$

$$\frac{\partial B_z}{\partial t} = \frac{\partial E_x}{\partial y} - \frac{\partial E_y}{\partial x}$$

$$\frac{\partial D_x}{\partial t} = \frac{\partial H_z}{\partial y} - \frac{\partial H_y}{\partial z} - J_x$$

$$\frac{\partial D_y}{\partial t} = \frac{\partial H_x}{\partial z} - \frac{\partial H_z}{\partial x} - J_y$$

$$\frac{\partial D_z}{\partial t} = \frac{\partial H_y}{\partial x} - \frac{\partial H_x}{\partial y} - J_z$$

discretization of equations

$$\frac{B^{n+\frac{1}{2}}_{x;\,i,j+\frac{1}{2},k+\frac{1}{2}} - B^{n-\frac{1}{2}}_{x;\,i,j+\frac{1}{2},k+\frac{1}{2}}}{\Delta t} = \frac{E^{n}_{y;\,i,j+\frac{1}{2},k+1} - E^{n}_{y;\,i,j+\frac{1}{2},k}}{\Delta z} - \frac{E^{n}_{z;\,i,j+1,k+\frac{1}{2}} - E^{n}_{z;\,i,j,k+\frac{1}{2}}}{\Delta y}$$

$$\frac{D^{n}_{x;\,i+\frac{1}{2},j,k} - D^{n-1}_{x;\,i+\frac{1}{2},j,k}}{\Delta t} = \frac{H^{n-\frac{1}{2}}_{z;\,i+\frac{1}{2},j+\frac{1}{2},k} - H^{n-\frac{1}{2}}_{z;\,i+\frac{1}{2},j-\frac{1}{2},k}}{\Delta y} - \frac{H^{n-\frac{1}{2}}_{y;\,i+\frac{1}{2},j,k+\frac{1}{2}} - H^{n-\frac{1}{2}}_{y;\,i+\frac{1}{2},j,k-\frac{1}{2}}}{\Delta z} - J^{n-\frac{1}{2}}_{x;\,i+\frac{1}{2},j,k}$$

meshing

Yee's cell

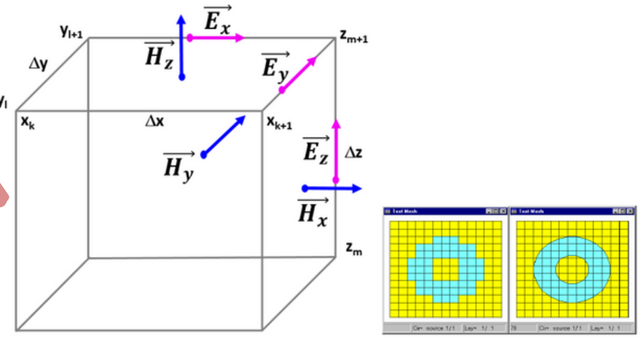

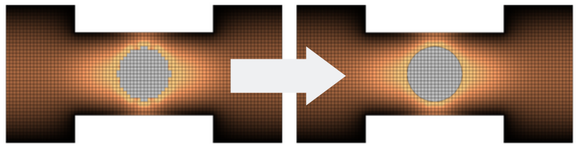

Conformal FDTD engine

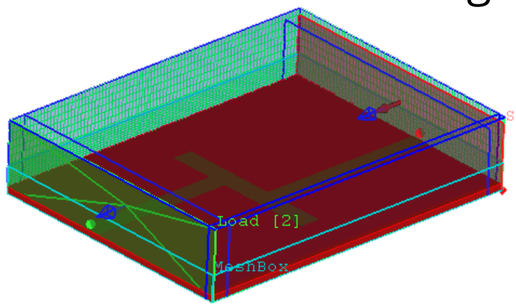

simulation

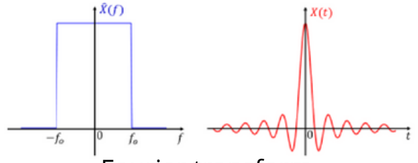

Fourier transform

$$v\Delta t \le 1/\sqrt{\frac{1}{(\Delta x)^2} + \frac{1}{(\Delta y)^2} + \frac{1}{(\Delta z)^2}}$$

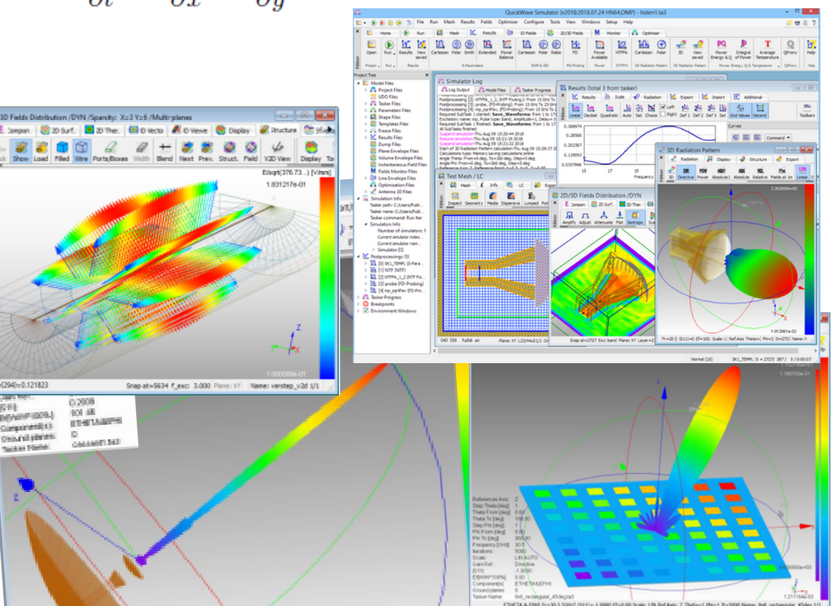

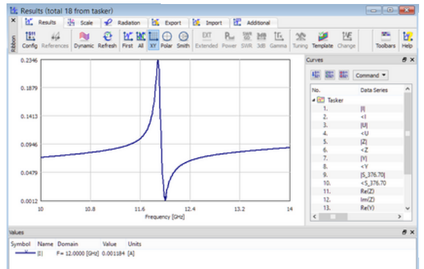

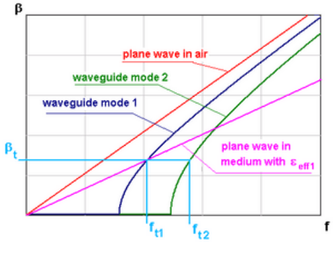

determination of the excitation field pattern

Modelling CPW in QuickWave

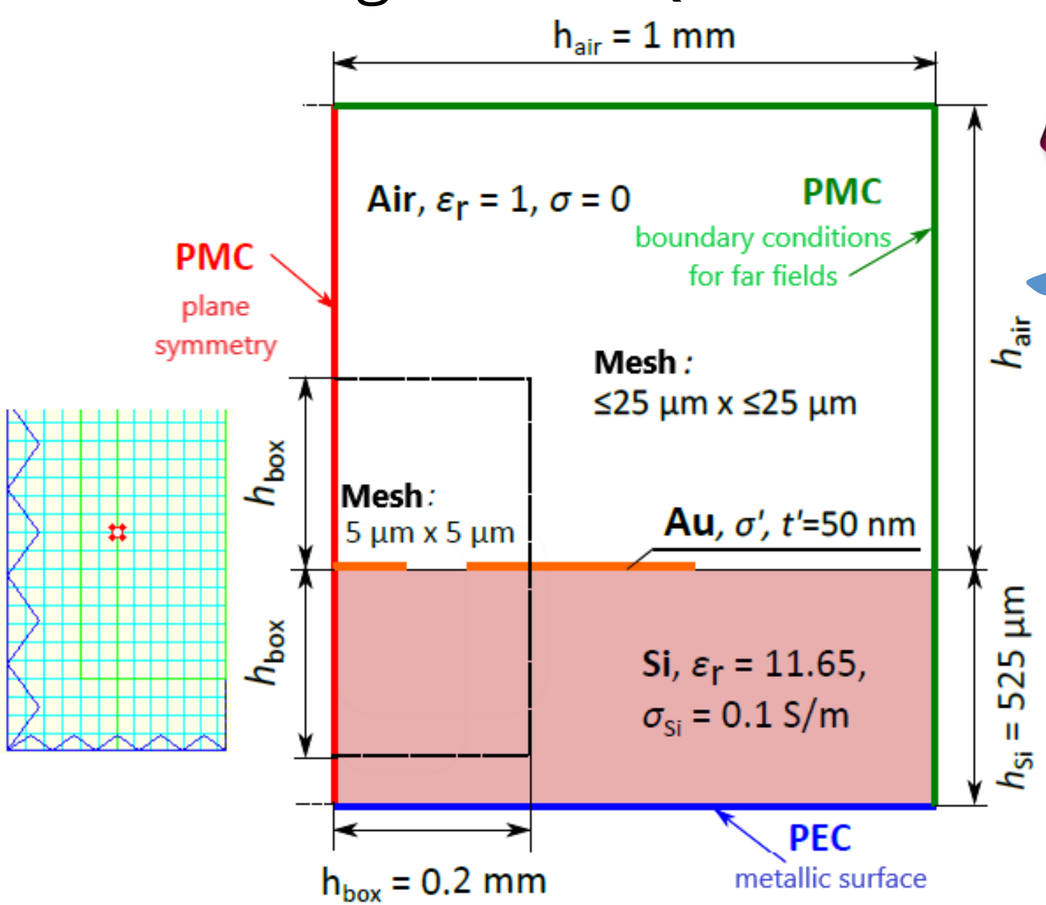

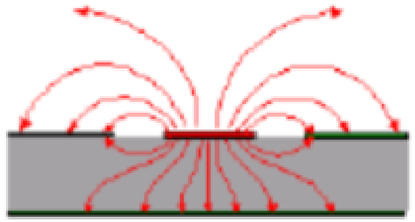

Design in QuickWave Modeller

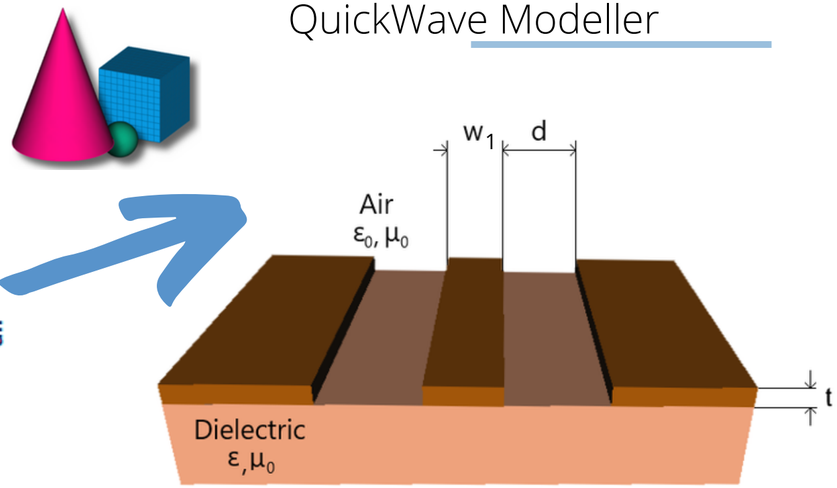

Model with measuring probes

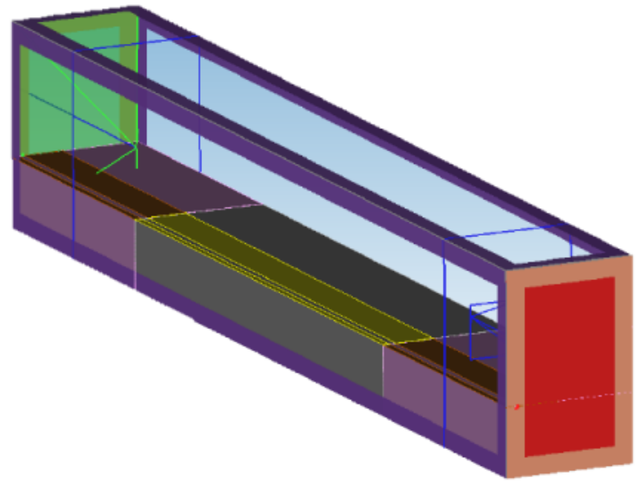

Assumptions:

- CPW length is equal to **4 mm**, measuring probes length is equal to **2 mm**
- The width of the outer strip is equal to W_2= **100 µm / 300 µm**
- Cell size: **5 µm x 5 µm x 100 µm / 25 µm x 25 µm x 100 µm**
- Excitation field patterns were generated for **f = 10 GHz**
- excitation pulse with a rectangular frequency spectrum from **0** to **26 GHz**, lasting **0.23** ns (about 23 000 iterations)
- Analysis of half waveguide due to its symmetry
- **PMC** and **PEC** boundary conditions
- Gold and chromium coplanar strips were treated as one with averaged conductivity $t = t_{Au} + t_{Cr}$
- The silicon substrate was assumed to be homogeneous and isotropic
- Maintains the condition $\sigma \cdot t = \sigma' \cdot t'$

CPW modelling with the FDTD method

CPW with measuring probes

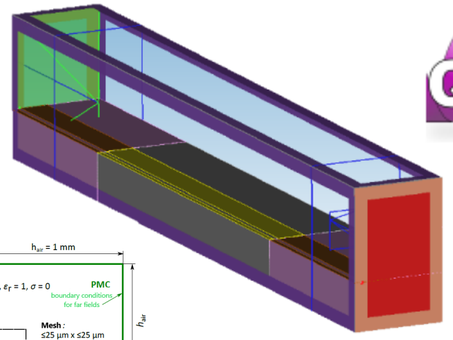

QuickWave [6]

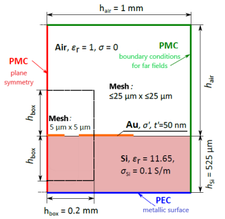

Design in QuickWave Modeller

Vector Network Analyzer

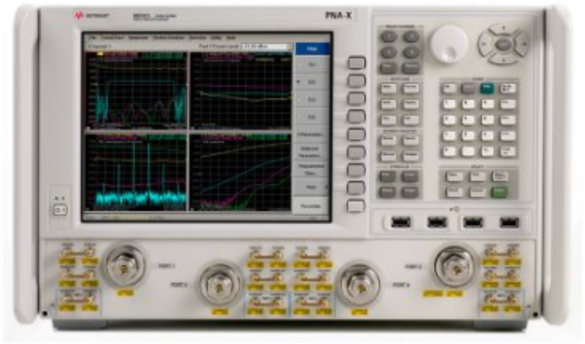

Agilent N5242A PNA-X [4][7]

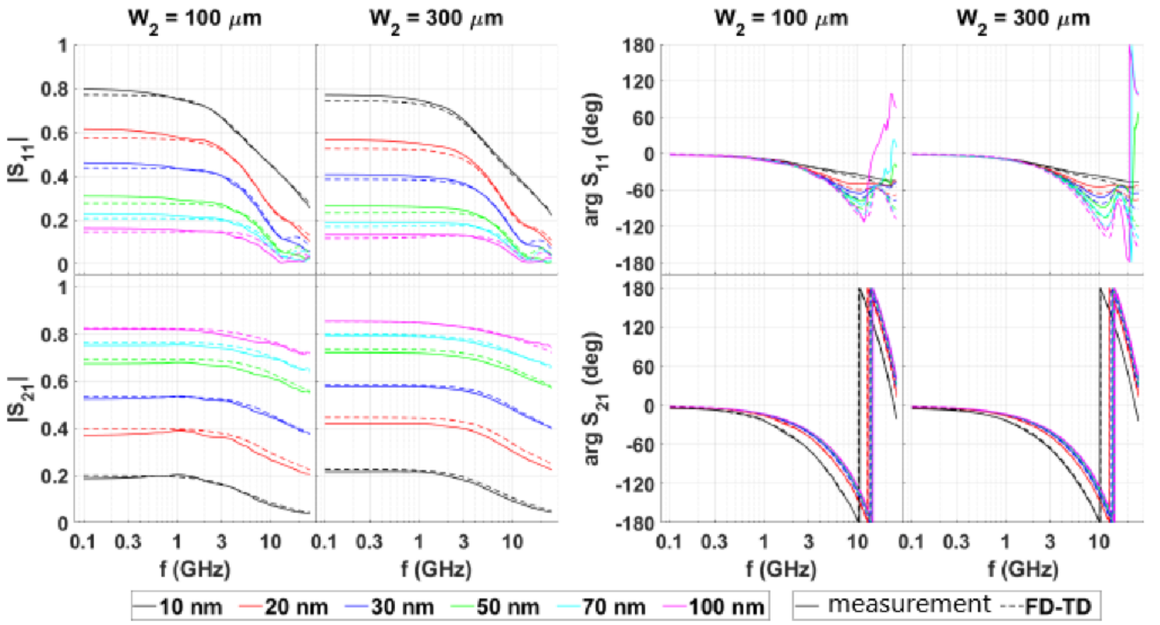

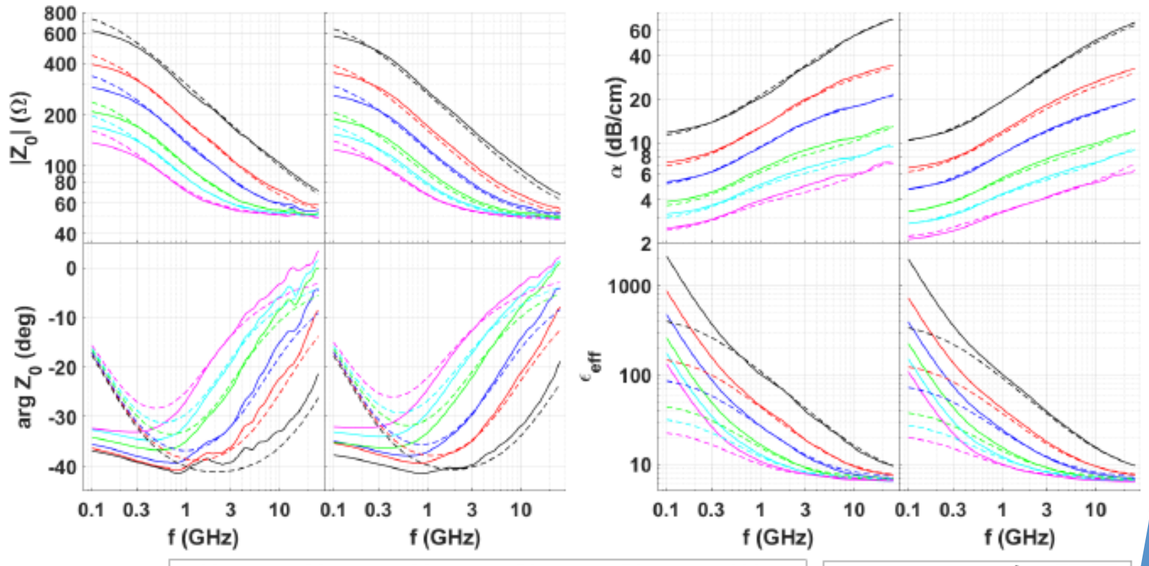

CPW modelling with the FDTD method

Convergence tests

Scaterring Matrix

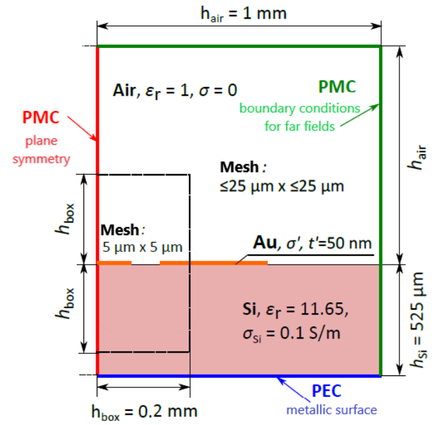

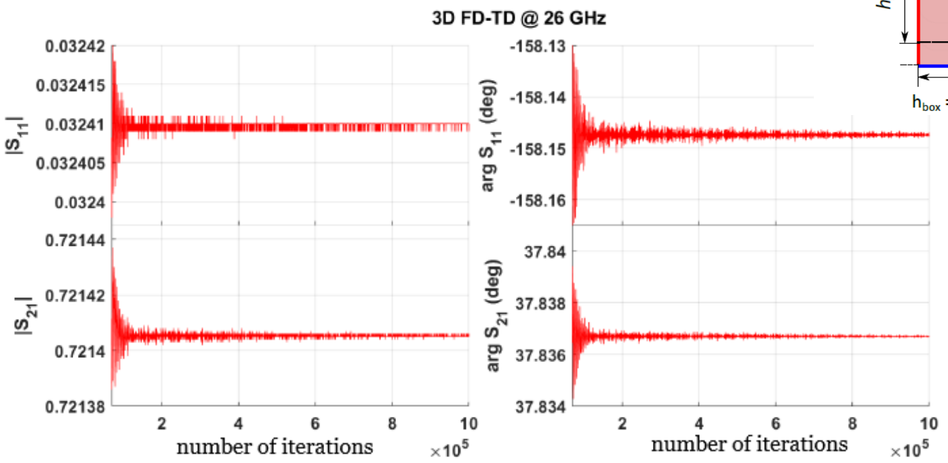

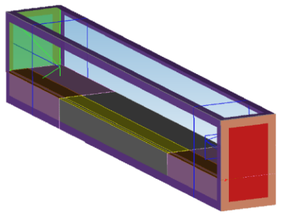

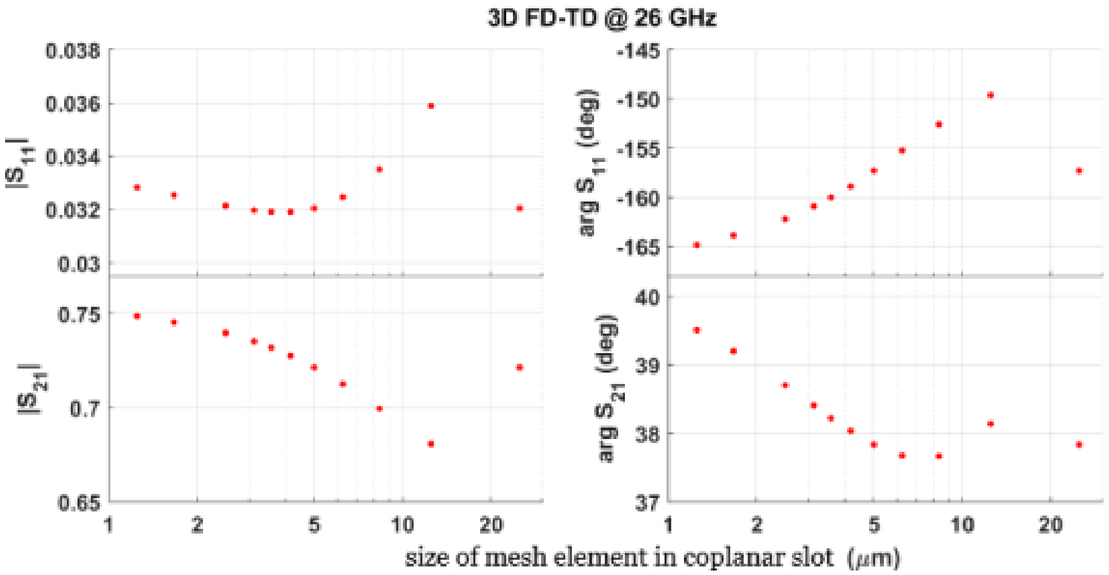

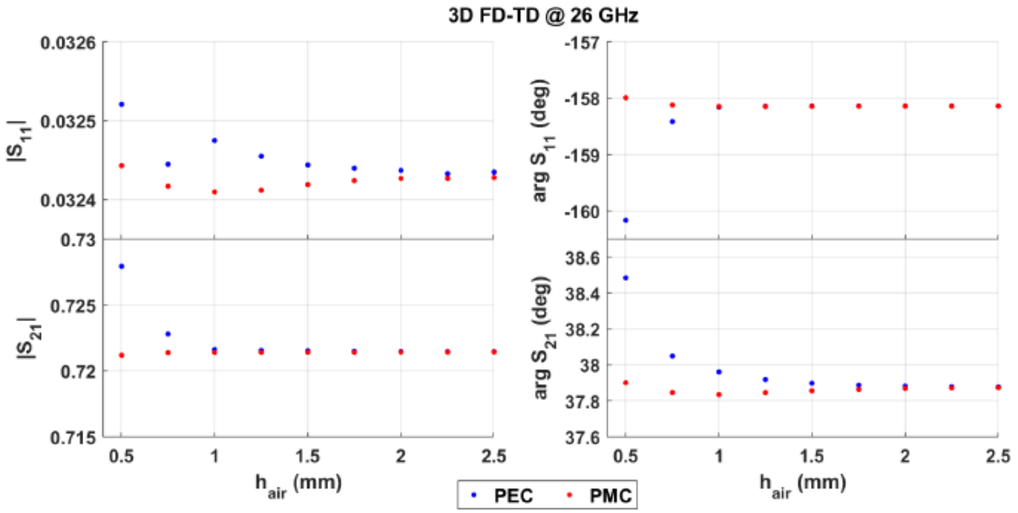

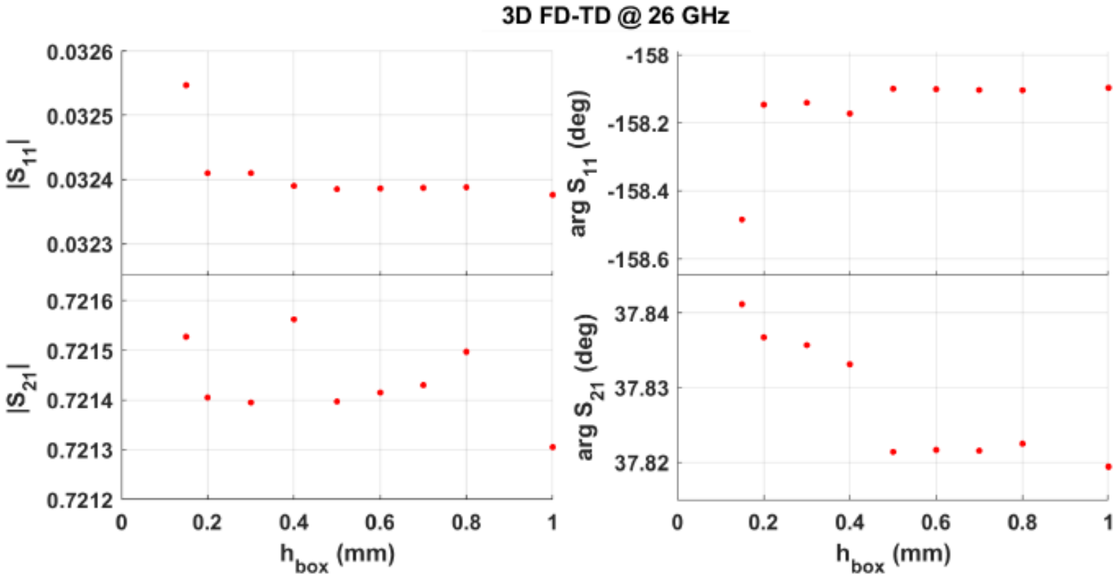

CPW modelling with the FDTD method

Convergence tests

Scaterring Matrix

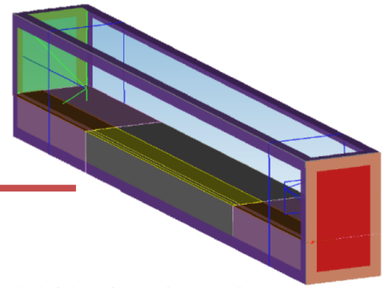

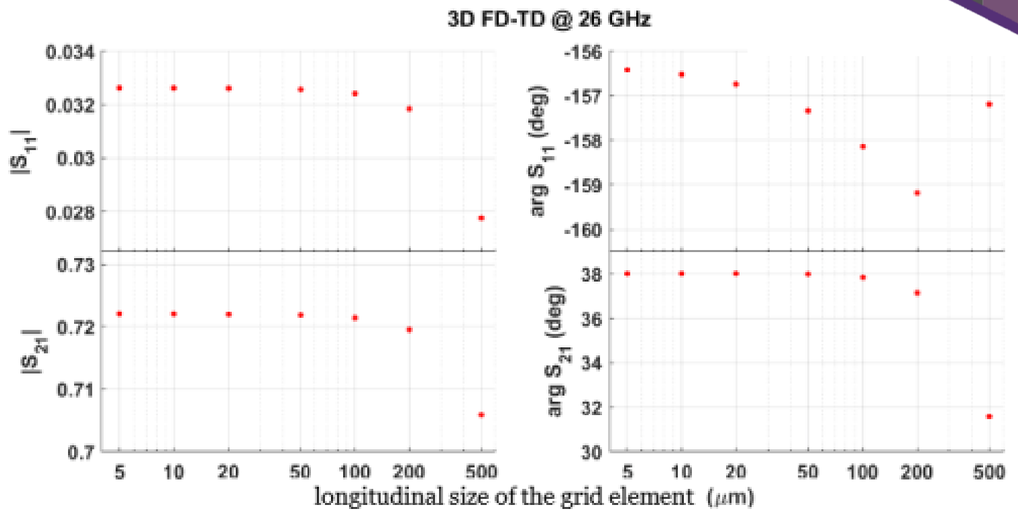

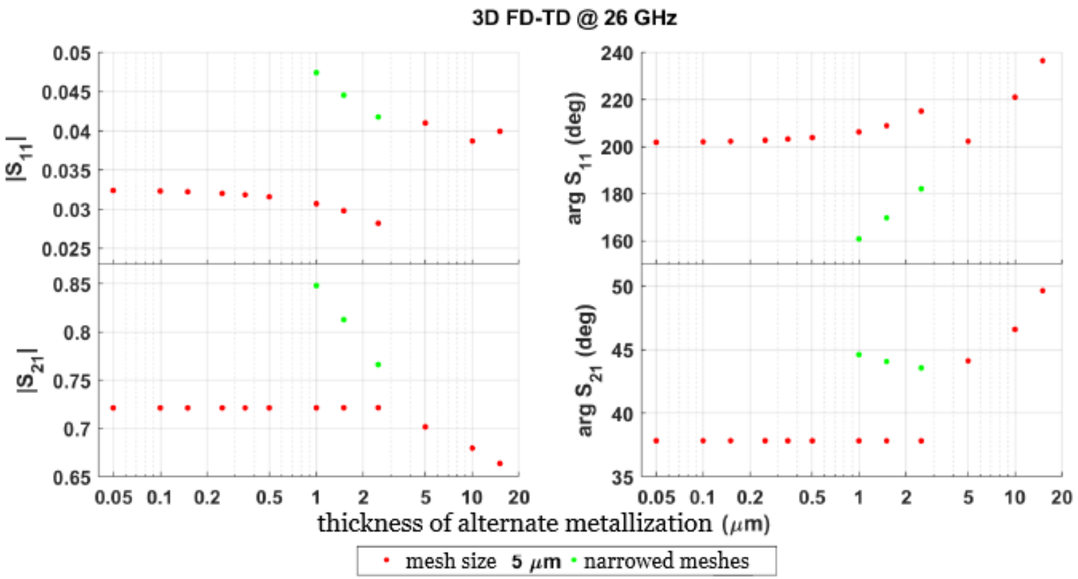

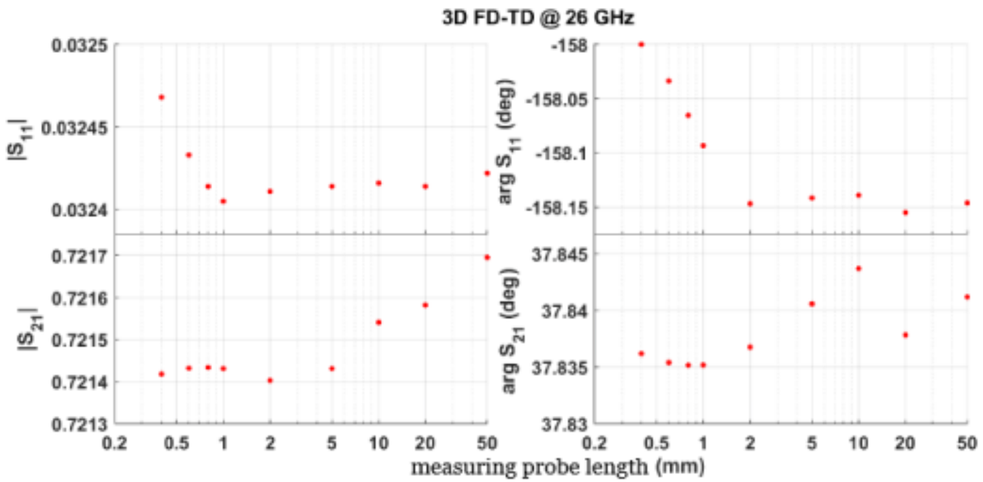

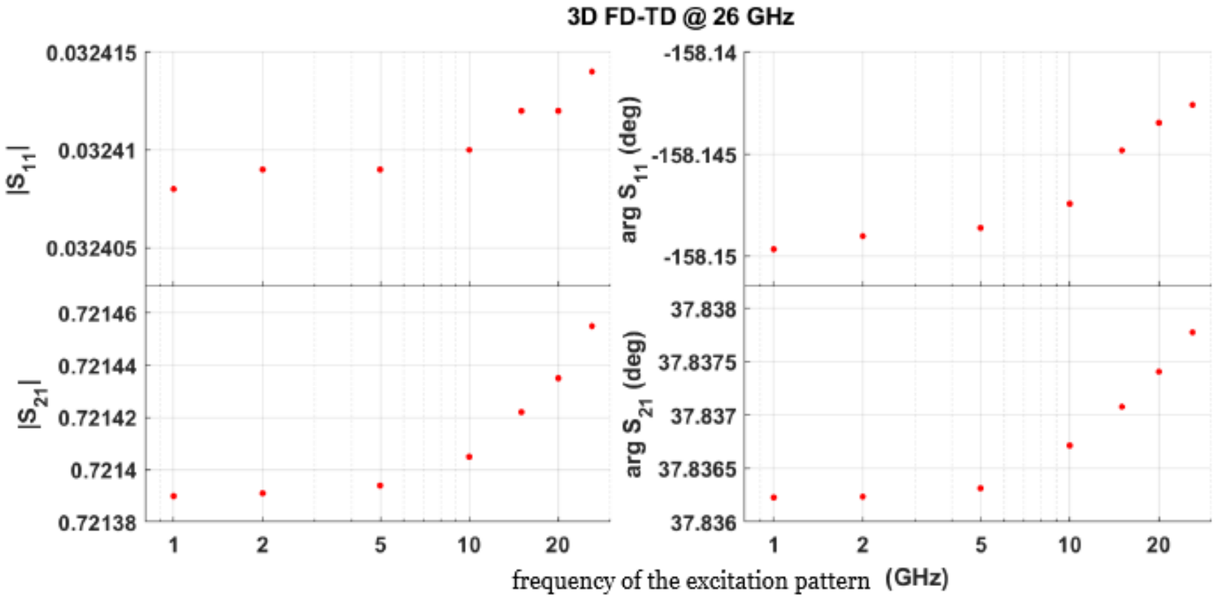

Convergence tests

Characteristic parameters

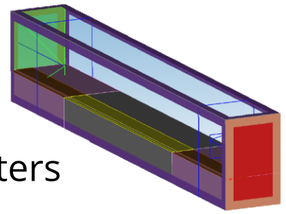

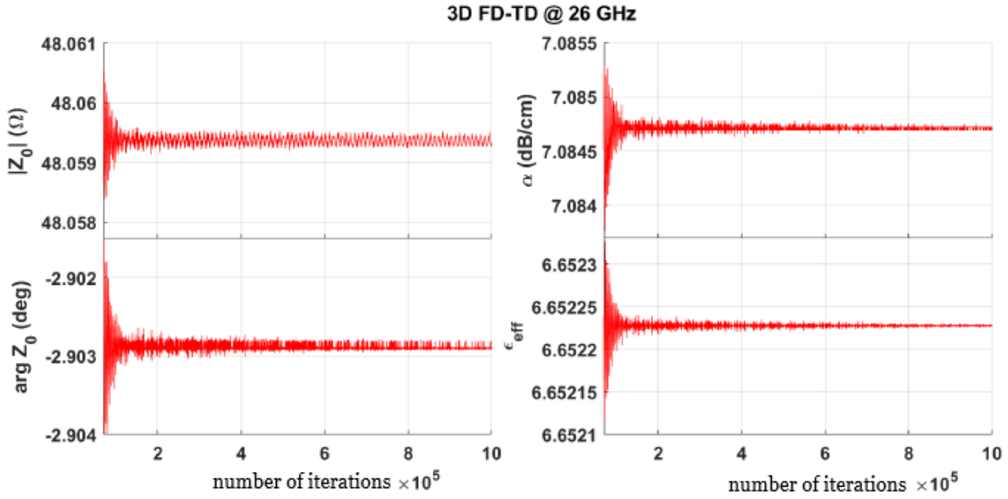

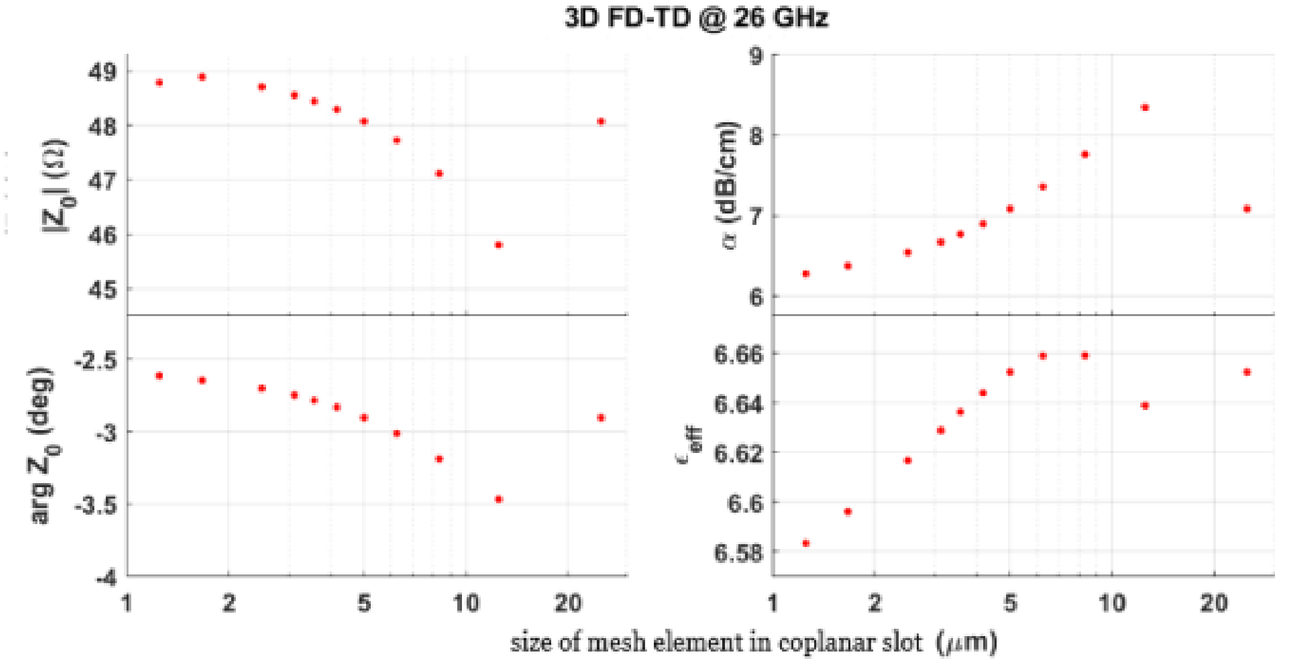

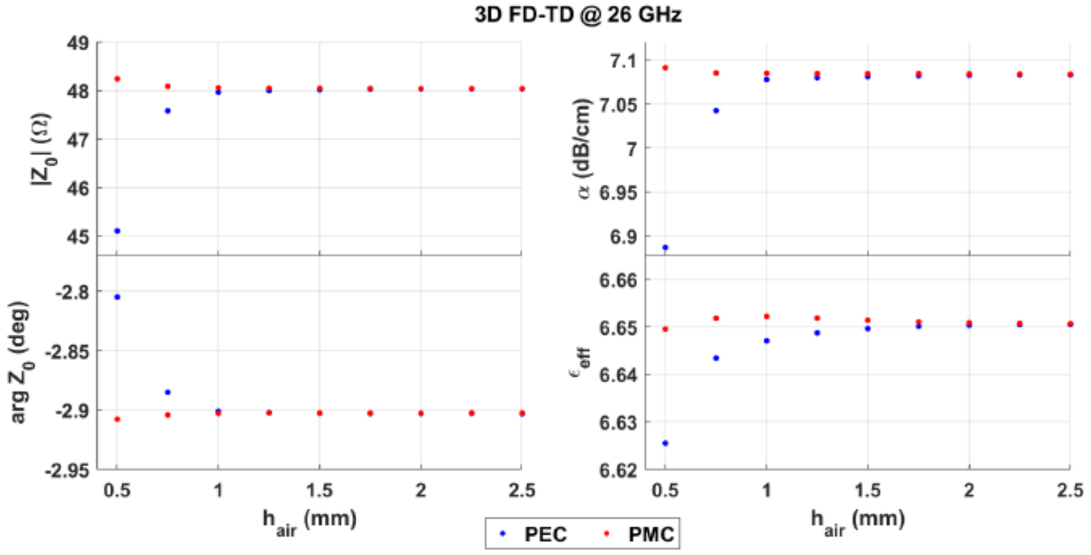

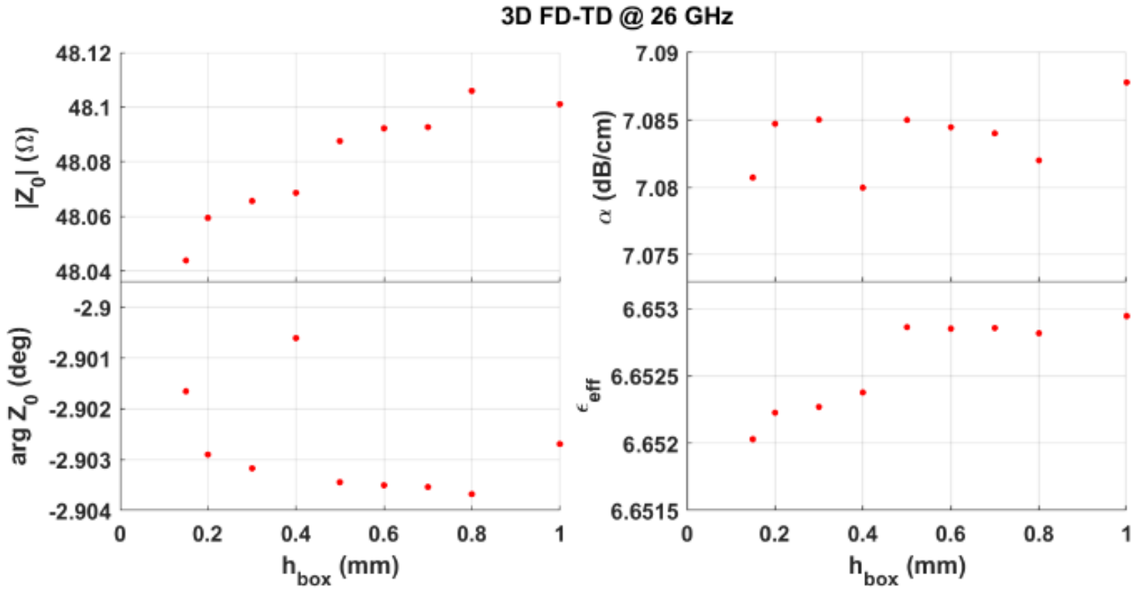

CPW modelling with the FDTD method

Convergence tests

Characteristic parameters

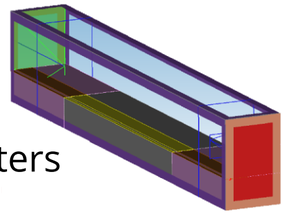

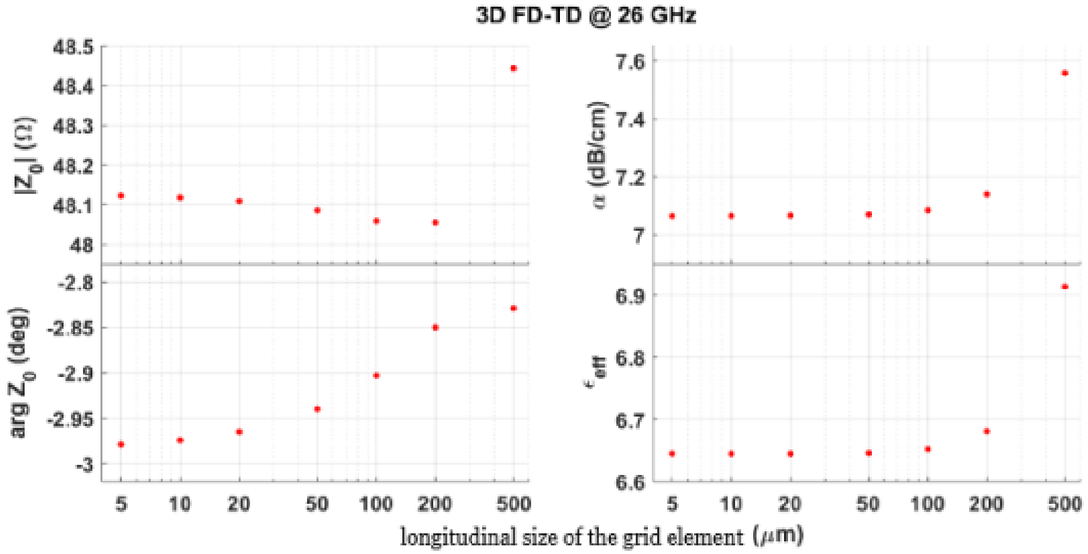

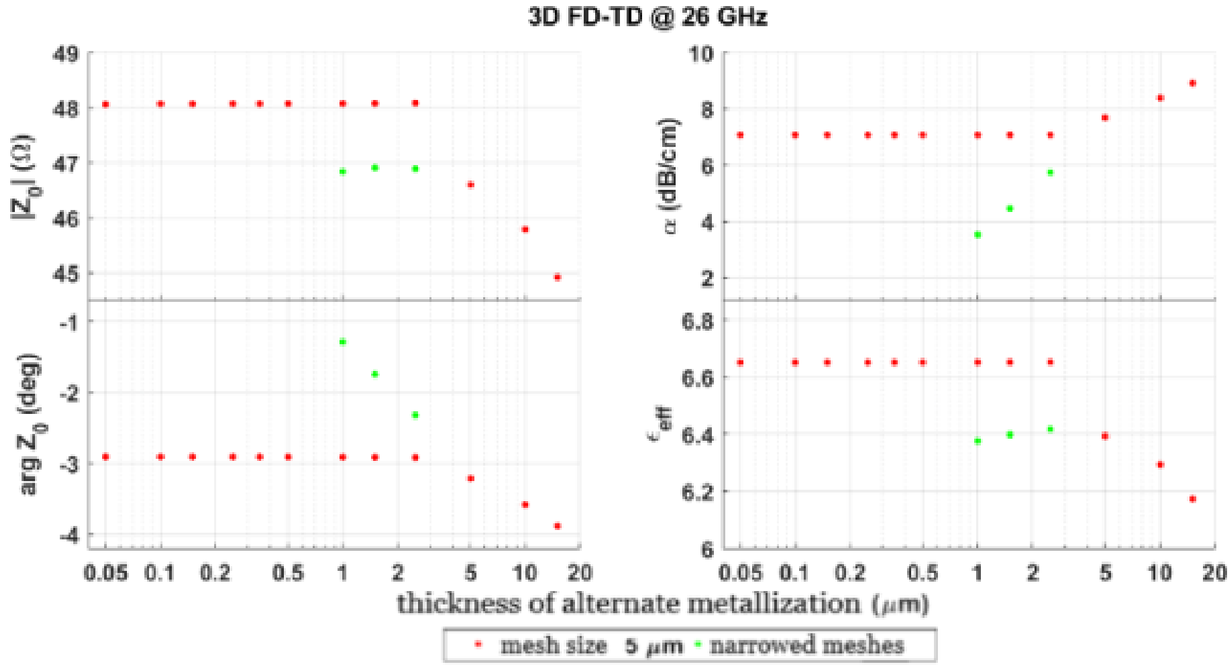

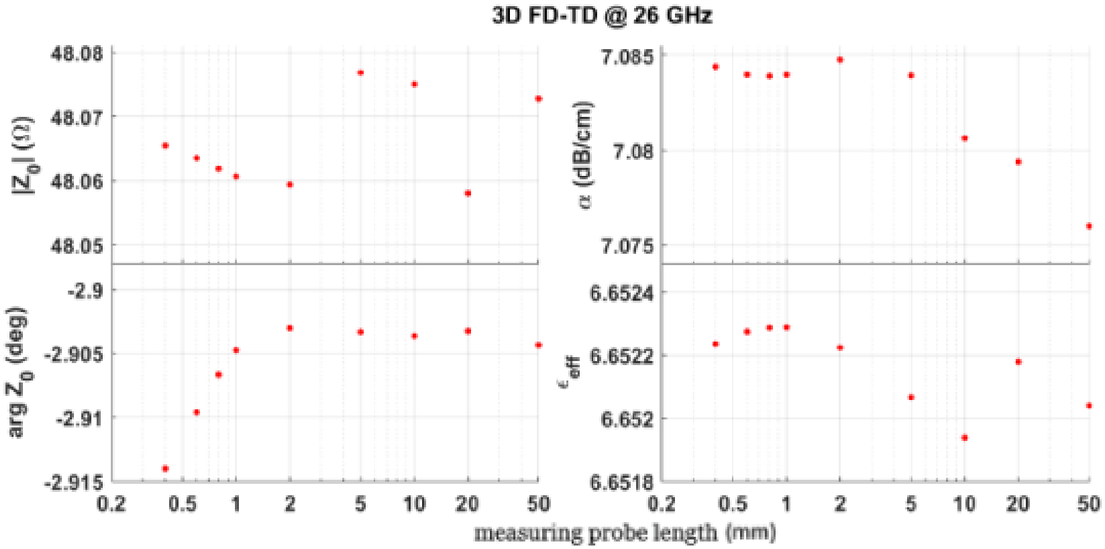

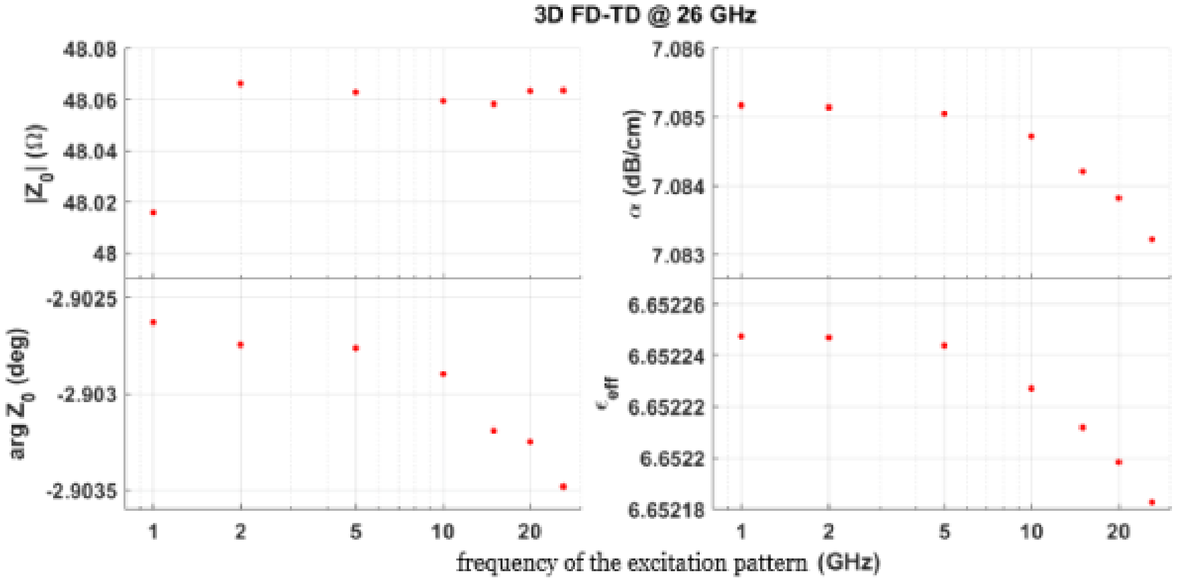

CPW modelling with the FDTD method

Convergence tests

Comparison

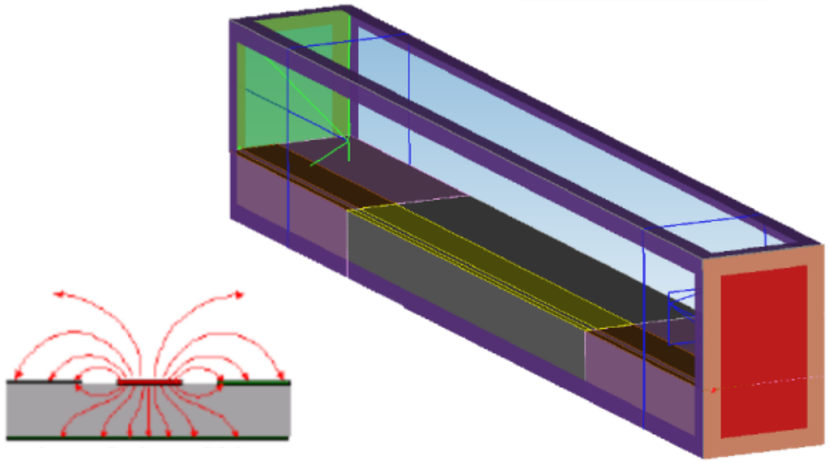

parameter	$\Delta\lvert S_{11}\rvert$	$\Delta \arg S_{11}$	$\Delta\lvert S_{21}\rvert$	$\Delta \arg S_{21}$
number of iterations	±0.000002	±0.003°	±0.000003	±0.0003°
space size h_{air}	-0.00002	-0.01°	-0.00005	-0.04°
transverse mesh size	—	10°	-0.04	—
size h_{box}	0.00003	±0.05°	±0.0002	0.015°
longitudinal mesh size	-0.0002	-2°	-0.0007	-0.16°
measuring probe lenght	Fluctuations increase with the length of the probe			
thickness of alternate metallization	±0.0002	±0.2°	±0.00003	±0.0007°
frequency of the excitation pattern	-0.000005	-0.005°	-0.00005	-0.001°

parameter	$\Delta\lvert Z_0\rvert$ (Ω)	$\Delta \arg Z_0$ (°)	$\Delta\alpha$ (dB/cm)	$\Delta\varepsilon_{eff}$
number of iterations	±0.0002	±0.0002	±0.0001	±0.00001
space size h_{air}	0.02	±0.0005	0.0015	0.0015
transverse mesh size	-1	-0.5	1	—
size h_{box}	-0.04	±0.0025	±0.004	-0.001
longitudinal mesh size	-0.07	0.08	0.02	0.007
measuring probe lenght	Fluctuations increase with the length of the probe			
thickness of alternate metallization	±0.012	±0.0003	±0.0005	±0.00005
frequency of the excitation pattern	-0.004	0.0007	0.0015	0.00005

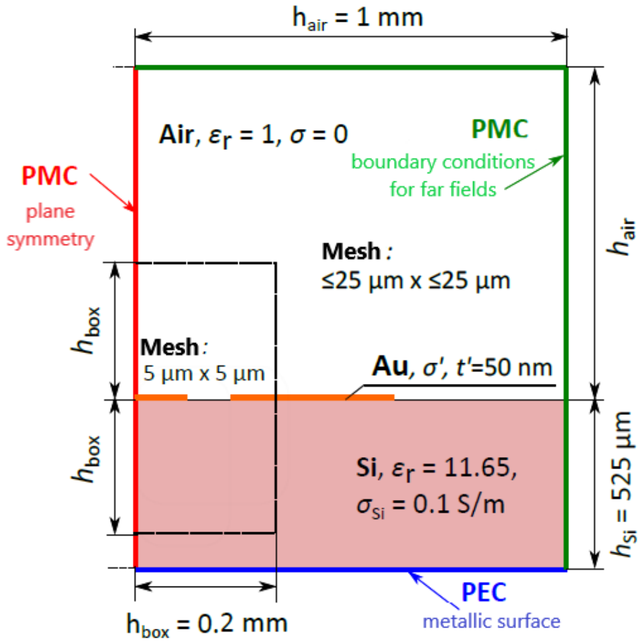

How does one efficiently model a layer of ultra-small thickness in general purpose EM simulators?

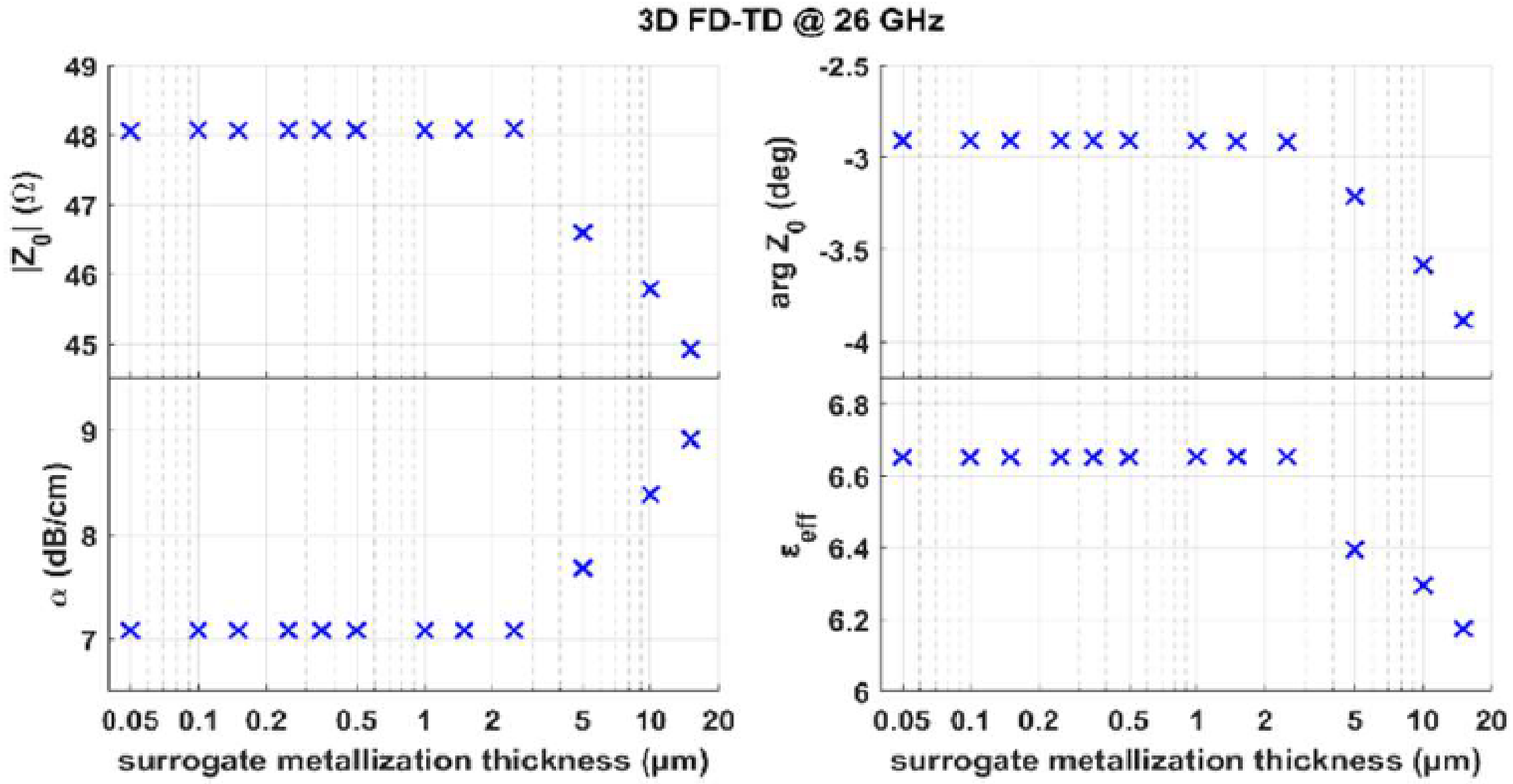

$$R_s = (d_0 \sigma_0)^{-1} = (d\,\sigma)^{-1}$$

parameters of the original metal

dielectric surrogate

Simulated parameters of CPW after [4] (case of W2=300 μm, Rs=0.326 [Ω/□], thickness 100 nm Au + 5nm Cr) at 26 GHz, with uniform FDTD meshing of 5 μm, as a function of scaled surrogate thickness – in pefect agreement with the measurements of [4] for surrogate thicknesses below 2.5 μm and ca. 2% impedance error for thickness equal to the FDTD cell size.

Application of the model to development of a 10 GHz DR scanner for graphene anodes.

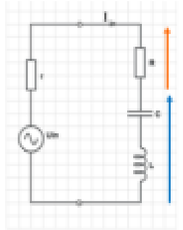

given fixed strength of Uin,
at resonance U_R is strongest (U_{LC}=0)

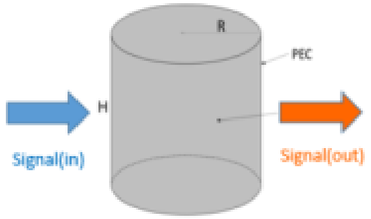

given fixed strength of Signal(in),
at resonance Signal (out) is strongest

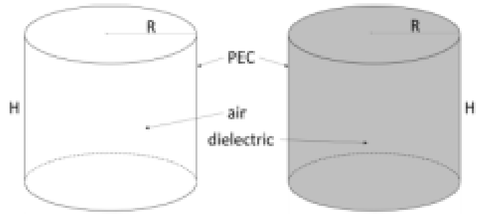

$$f_{r,mnp} = \frac{c}{\sqrt{Dk}}\sqrt{\left(\frac{\kappa_{mn}^{(.)}}{\pi R}\right)^2 + \left(\frac{p}{H}\right)^2}$$

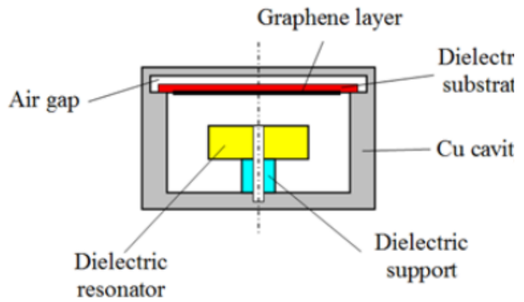

Cross section of the resonator for graphene measu

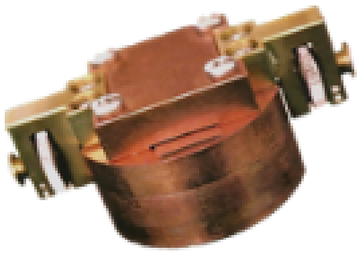

$$Q = 2\pi \frac{\iiint_V \varepsilon \vec{E}\cdot\vec{E}^* dv}{T\iiint_V \sigma \vec{E}\cdot\vec{E}^* dv} = \frac{\omega\varepsilon}{\sigma} = \frac{1}{Df} \approx \frac{fres}{\Delta f}$$

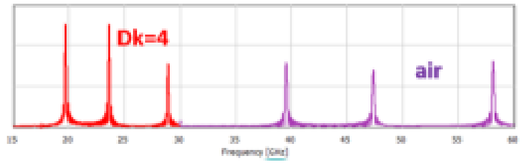

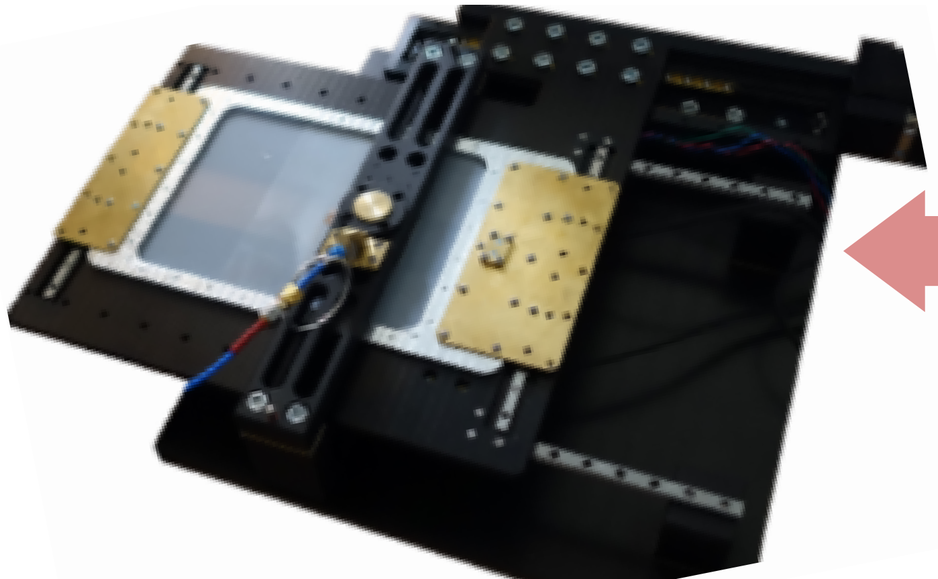

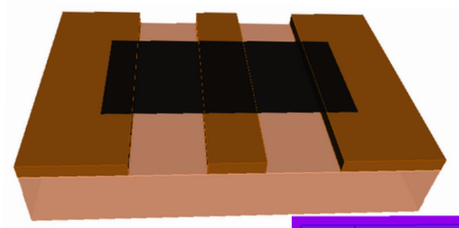

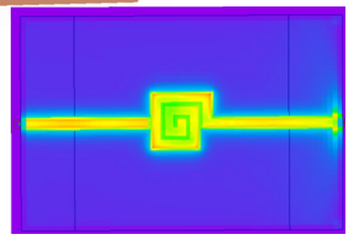

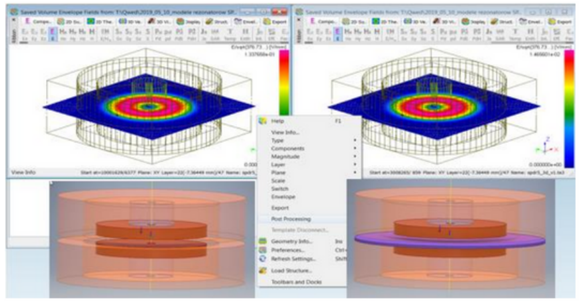

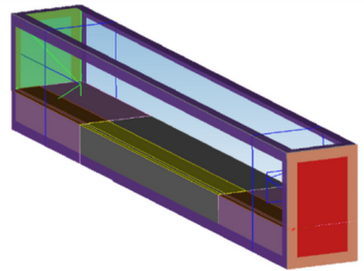

Application of the model to development of a 10 GHz DR scanner for graphene anodes.

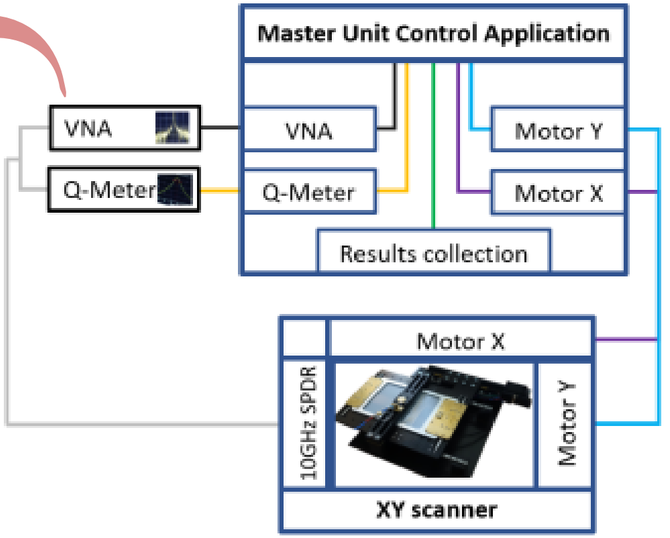

Nano Bat

Graphene anodes (*PLEIONE, Greece*)

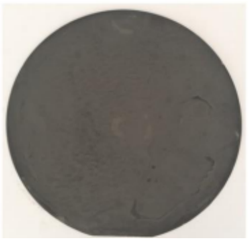

Sample		Surface resistance [Ω/□]
GNP on quartz	Edge	21.485
	Centre	21.020
GNP on polymer	Edge	90.167
	Centre	25.557

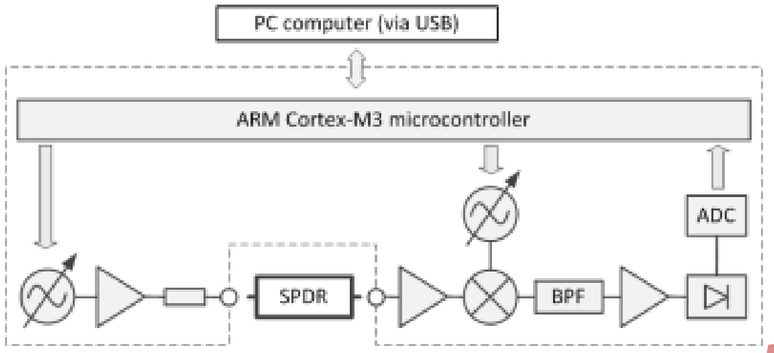

Q-Meter

Conclusions

In this work, simulations of a benchmark CPW structure with ultra-thin metalization made of gold thickness on a substrate of high-resistivity silicon for the frequency of 26 GHz

- Behind every **CHARACTERISATION** there is always a **MODEL**
- **Rs** parameter unambiguously determines the characteristic impedance, propagation constant, and effective permittivity of transmission lines with **ultra-thin** (<110 nm) signal and ground-plane layers.
- extensive study has been conducted for the convergence and accuracy of FDTD models of **CPW**-based material test-fixtures. For the thin films, a lossy dielectric **surrogate** preserving **Rs** = $(d\ \sigma)^{-1}$ has been shown most efficient and valid up to the thickness of one **FDTD** cell (with cell size dictated by the **CPW** geometry and frequency range).
- Attenuation coefficient is directly and inversely dependent on the metallization thickness
- For more information about **DR** come today to Amphi 400C at **17:35**

Acknowledgement

For authors:

Malgorzata Celuch **&** Marzena Olszewska – Placha **&** Konrad Wilczynski

The work presented has received funding from

NanoBat aims to develop a novel **nanotechnology** toolbox for quality testing of Li-ion and beyond **Lithium batteries**.

The work of **QWED** is supported by the European Union's **Horizon 2020** research and innovation programme under grant agreement NanoBat **no. 861962.**

Foundation for Polish Science

an independent, non-profit making organisation which aim at improving the opportunities for doing research in Poland.

Fundusze Europejskie Inteligentny Rozwój

The work of **K. Wilczynski** was supported by the FNP **Team-Tech** project No. POIR.04.04.00-00-3C25/16-00.

REFERENCES

[1] P. C. Theofanopoulos and G. C. Trichopoulos, “Modeling and analysis of Terahertz graphene switches for on-wafer coplanar transmission lines”, J. Infrared, Millimeter, Terahertz Waves, vol. 41, pp. 758 775, 2020.

[2] Masouras, D. Giannopoulos, B. Hasa, and A. Katsaounis, V. Kostopoulos, “Hybrid graphene nanoplatelet/manganese oxide electrodes for solid-state supercapacitors and application to carbon fiber composite multifunctional materials”, J. Energy Storage, vol. 2019, pp. 515-525, 2019.

[3] M. Celuch, K. Wilczynski, and M. Olszewska-Placha, ”Generalisation and evaluation of macroscopic models for microwave susceptors in contact with heated foods”, 17th Intl. Conf. on Microwave and High Frequency Heating AMPERE, Sep. 2019, DOI: http://dx.doi.org/10.4995/Ampere2019.2019.9847

[4] J. Judek, A. P. Gertych, M. Swiniarski, M. Zdrojek, J. Krupka, and J. K. Piotrowski, “Characterization of finite-width ground coplanar waveguides on high resistivity silicon with ultralow metallization thickness,” IEEE Trans. Microw. Theory Tech., vol. 65, no. 12, pp. 4836–4842, 2017.

[5] M. Celuch, J. Rudnicki, J. Krupka, and W. Gwarek, "Application of dielectric resonators to surface impedance measurements of microwave susceptors", 17th Intl. Conf. on Microwave and High Frequency Heating AMPERE, Sep. 2019, DOI: http://dx.doi.org/10.4995/Ampere2019.2019.9953 .

[6] K. Wilczyński, “Modelling of parameters of finite-width ground coplanar waveguides on high resistivity silicon with ultra-low metallization thickness using FEM and FD-TD methods” (in Polish), M.Sc. Thesis, Faculty of Physics, Warsaw Univ. of Technology, Poland, 2019.

[7] https://www.keysight.com/us/en/product/N5242A/pnax-microwave-network-analyzer-265-ghz.html

[8] Six techniques for measuring dielectric properties, newelectronics.co.uk/electronics-technology/six-techniques-for-measuring-dielectric-properties/152591/, Access: 21/06/2019.

Thank You